

TIDALLY-TRIGGERED STAR FORMATION IN CLOSE PAIRS OF GALAXIES 2: CONSTRAINTS ON BURST STRENGTHS AND AGES

ELIZABETH BARTON GILLESPIE¹

University of Arizona, Steward Observatory, 933 N. Cherry Ave., Tucson, AZ 85721 (email: bgillespie@as.arizona.edu)

AND

MARGARET J. GELLER, SCOTT J. KENYON

Smithsonian Astrophysical Observatory, 60 Garden St., Cambridge, MA 02138 (email: mgeller,skenyon@cfa.harvard.edu)

Draft version November 26, 2018

ABSTRACT

Galaxy-galaxy interactions rearrange the baryons in galaxies and trigger substantial star formation; the aggregate effects of these interactions on the evolutionary histories of galaxies in the Universe are poorly understood. We combine B and R -band photometry and optical spectroscopy to estimate the strengths and timescales of bursts of triggered star formation in the centers of 190 galaxies in pairs and compact groups. Based on an analysis of the measured colors and $\text{EW}(\text{H}\alpha)$, we characterize the pre-existing and triggered populations separately. The best-fitting burst scenarios assume stronger reddening corrections for line emission than for the continuum and continuous star formation lasting for \gtrsim a hundred Myr. The most realistic scenarios require an initial mass function that is deficient in the highest-mass stars. The color of the pre-existing stellar population is the most significant source of uncertainty.

Triggered star formation contributes substantially (probably $\gtrsim 50\%$) to the R -band flux in the central regions of several galaxies; tidal tails do not necessarily accompany this star formation. Many of the galaxies in our sample have bluer centers than outskirts, suggesting that pre- or non-merger interactions may lead to evolution along the Hubble sequence. These objects would appear blue and compact at higher redshifts; the older, redder outskirts of the disks would be difficult to detect. Our data indicate that galaxies with larger separations on the sky contain weaker, and probably older, bursts of star formation on average. However, confirmation of these trends requires further constraints on the colors of the older stellar populations and on the reddening for individual galaxies.

Subject headings: galaxies: evolution — galaxies: fundamental parameters — galaxies: kinematics and dynamics — galaxies: interactions — galaxies: structure

1. INTRODUCTION

Larson & Tinsley (1978) showed that galaxies in pairs exhibit a broader scatter in the $U - B/B - V$ plane than “field” galaxies, demonstrating that interactions trigger bursts of star formation. Since then, numerous studies, both of statistical samples and of individual interacting systems, have confirmed their results (e.g., Kennicutt & Keel 1984; Madore 1986; Kennicutt et al. 1987; Jones & Stein 1989; Sekiguchi & Wolstencroft 1992; Keel 1993; Liu & Kennicutt 1995a,b; Keel 1996; Donzelli & Pastoriza 1997; Barton, Geller, & Kenyon 2000a). These studies have conclusively established the link between interactions and star formation. However, many questions remain about the true role of interactions in the evolutionary history of galaxies in the Universe.

Because interaction timescales are much shorter than a Hubble time, galaxies may participate in many interactions and/or mergers during their lifetimes. The strengths and durations of typical triggered bursts of star formation are therefore important cosmological parameters. An understanding of interactions is a necessary basis for including interactions and mergers in models of galaxy formation (e.g., Somerville & Primack 1999; Diaferio et al. 1999; Kauffmann et al. 1999a,b). Studies of local interactions also aid interpretation of the unusual morphologies and structural parameters of intermediate redshift galaxies (e.g., Koo et al. 1994; Abraham et al. 1996; Barton & van Zee 2001). Finally, a measure of the total effects of interaction may yield constraints on the causes of evolution along the Hubble sequence; large amounts of gas funneled into the cen-

ters of the galaxies could result in interaction-induced forms of the processes in secular evolution (Pfenniger & Norman 1990) that cause the formation of “exponential bulges” (Andredakis & Sanders 1994; Carollo 1999).

Barton, Geller, & Kenyon (2000a, BGK hereafter) study 502 galaxies in pairs or compact groups selected from the CfA2 redshift survey. They find a significant correlation between pair separation on the sky, ΔD , and $\text{H}\alpha$ equivalent width, $\text{EW}(\text{H}\alpha)$. The correlation also extends to the $\Delta V/\text{EW}(\text{H}\alpha)$ plane, where ΔV is the pair separation in velocity. BGK argue that the $\Delta D - \text{EW}(\text{H}\alpha)$ correlation results from the aging of a continuing burst of star formation. If their interpretation is correct, the correlation provides a method of measuring the durations and initial mass functions (IMFs) of the bursts by comparing dynamical timescales with star-formation timescales. Here we investigate the origin of this correlation by using B and R photometry to constrain the old stellar population and the new burst of star formation separately.

To measure the amount and current age of the new burst of star formation, we explore a method of using the measured colors and $\text{EW}(\text{H}\alpha)$ to characterize recent star formation superposed on a pre-existing stellar population. We relate these quantities to the orbital parameters of the pairs, thus exploring the origin of the BGK correlation. In Sec. 2 we describe the pair sample and the data. Sec. 3 contains a description of the “two-population” model we apply to characterize the burst of star formation independent of the underlying older stellar population. We include a brief discussion of the results of applying the model to the data. We discuss the origin of the BGK $\Delta D - \text{EW}(\text{H}\alpha)$ correlation in Sec. 4. In Sec. 5 we explore the depen-

¹ Hubble fellow.

dence of burst strength and age on the R-band luminosities and rotation speeds of the galaxies. We describe the galaxies with strong bursts of central star formation in Sec. 6 and conclude in Sec. 7.

2. THE PAIR SAMPLE

We base our study on the sample of all 786 galaxies in pairs and compact groups drawn from the original CfA2 redshift survey ($m_{Zw} \leq 15.5$) with $\Delta D \leq 50 \text{ h}^{-1} \text{ kpc}$, $\Delta V \leq 1000 \text{ km/s}$ and $v \leq 2300 \text{ km/s}$, where ΔV is the pair (or compact group neighbor) velocity separation, and $v = cz$ is the apparent recession velocity. BGK estimate that this “full” sample of 786 galaxies from the original CfA2 survey is 70% complete with respect to all known galaxies in pairs over the region of interest in the updated CfA2 redshift survey (Falco et al. 1999). 41 of the 502 galaxies with (new) spectra fail to satisfy the original selection criteria. We include these galaxies in the analysis because most come close to satisfying the criteria; all pairs in the sample satisfy $\Delta D < 77 \text{ h}^{-1} \text{ kpc}$ and $\Delta V < 1035 \text{ km/s}$.

We divide the full sample into three overlapping sub-samples for which we have different kinds of data: the dynamical sample (~ 140 galaxies, mostly spirals and S0s, with $H\alpha$ rotation curves), the spectroscopic sample (502 galaxies with one-dimensional spectra; the same as the BGK sample) and the photometric sample (196 galaxies with calibrated photometric images in B and R).

In this paper, we concentrate on the photometric properties of the galaxies in the overlap of the spectroscopic and photometric samples (190 galaxies comprising all or part of 78 pairs and 13 compact groups; SP sample hereafter). We have $H\alpha$ rotation curves for 103 of these galaxies; 89 provide useful measurements of V_c , the velocity width. BGK separate the sample into galaxies residing in low- and high-density environments and concentrate on the low-density subset to avoid contamination by the morphology-density relation and gas stripping in clusters. Here our sub-samples are much smaller and we are unable to divide the data in this way. However, we use direct measurements of V_c to understand the galaxy mass-dependent effects.

In spite of the $m_{Zw} \leq 15.5$ cutoff, the pair sample contains numerous galaxies with B magnitudes > 15.5 . These systems were often recorded in the CGCG (Zwicky & Kowal 1968), and therefore the redshift catalog, with the Zwicky magnitude of the whole system instead of separate magnitudes for each of the galaxies. We find 33 (of 190) galaxies (17%) with $m_{B26} > 15.5$ in the SP sample, where m_{B26} is the $\mu_B = 26$ isophotal magnitude. The sample is incomplete with respect to these galaxies.

We selected the systems in the dynamical sub-sample based on the suitability of at least one galaxy for a rotation curve measurement; therefore this sub-sample heavily favors $H\alpha$ -emitting galaxies and spirals less than $\sim 50^\circ$ from edge on. For the selection of the photometric and spectroscopic samples, we focus on (1) galaxies in the dynamical sample, and (2) galaxies known to have emission lines. Therefore, the SP sample heavily favors emission-line galaxies. We measure the extent of the bias by comparing the spectroscopic properties of the SP sample with those of the CfA2South pair sample, which is 100% complete with respect to the set of all pairs selected from the original CfA2 survey. Although only 25% of the complete CfA2South sample has detectable $EW(H\alpha)$, 75% of the (overlapping) SP sample has detectable $EW(H\alpha)$.

The SP sample does not favor line-emitting galaxies with

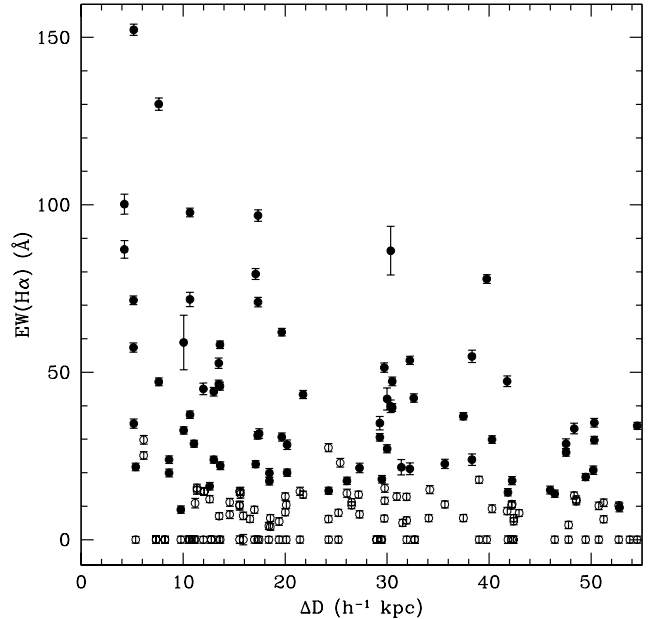


FIG. 1.— The relationship between ΔD and $EW(H\alpha)$ for the 190-galaxy SP sample (for comparison with BGK Fig. 2a). The trend is significant, with $P_{SR} = 0.058$ in the full SP sample and $P_{SR} = 0.0017$ in the sample restricted to galaxies with measured Balmer decrements (filled circles). We exclude 2 galaxies with $\Delta D > 55 \text{ h}^{-1} \text{ kpc}$ from the plot.

particularly strong emission. The distribution of $EW(H\alpha)$ in the line-emitting fraction of the SP sample is unbiased with respect to the $EW(H\alpha)$ distribution for the complete CfA2South sample; a K-S test is unable to detect differences in the $EW(H\alpha)$ distribution of galaxies with $EW(H\alpha) \geq 10 \text{ \AA}$ in the (overlapping) SP sample (115 galaxies) and the CfA2South spectroscopic samples (98 galaxies, with 44 in the SP sample), with $P_{KS} = 0.55$ including all galaxies, or $P_{KS} = 0.18$ excluding the overlapping galaxies. We plot ΔD vs. $EW(H\alpha)$ (uncorrected for reddening) for the SP sample in Fig. 1.

Differences are evident in the ΔD and redshift distributions of the SP and complete CfA2South samples. For example, the SP sample contains an excess of pairs with $\Delta D \sim 10 \text{ h}^{-1} \text{ kpc}$ and an excess of pairs at lower redshift. These effects result from the large-scale structure differences between CfA2North and CfA2South (see Falco et al. 1999). We use Spearman rank tests to evaluate the significance of the correlations we describe below. Therefore, the differences in the redshift and ΔD distributions should only have a significant bearing on our conclusions if we have different selection effects in different ranges of ΔD . We are not aware of any such effects.

2.1. Observations and Data Reduction

BGK and Barton et al. (2001) describe the basic observations and data reduction; we summarize these observations here and we list the results in Table 1.

We observed the galaxies at the FLWO 48" telescope on Mt. Hopkins through either Johnson or Harris B and Cousins or Harris R filters, for total exposure times of 15 minutes (usually spread over 3 images) and 5 minutes (usually exposed all at once or spread over 2 images), respectively. After calibrating the images to the Landolt (1992) standard-star system, we subtract the sky background and measure magnitudes and surface

TABLE 1
THE SP SAMPLE

Coordinates (1950)	N_{sys}	cz (km/s)	ΔD (kpc/h)	ΔV (km/s)	M_R	$(B-R)_s$	$EW(H\alpha)$ (Å)	$\frac{H\alpha}{H\beta}$	$V_{2.2}^c$ (km/s)	Note	Label
00 03 47.2 +17 09 05	2	5590	7.6	181	-19.94 ^{ab}	0.75	130.1	4.07		marg	
00 03 47.5 +17 09 32	2	5770	7.6	181	-20.14 ^{ab}	0.92	47.1	4.82	221.5	norm	
00 11 07.7 +47 52 24	2	5445	31.9	22	-21.40 ^{ac}	1.39	0.0	—			
00 11 19.5 +47 52 47	2	5422	31.9	22	-21.17 ^{ac}	1.51	5.8	—	372.6	norm	
00 17 52.0 -00 32 55	2	5222	9.8	423	-20.84 ^{ab}	1.38	9.0	2.88	247.9	marg	

^aImage was calibrated from a shorter exposure.

^bGalaxies overlapped.

^cBright star in background, or smaller but significant star(s) on galaxy.

Note. — Galaxies in the SP sample: (1) 1950 coordinates, (2) number of galaxies in system, (3) redshift, (4) separation of pair on the sky (or distance to closest galaxy in n-tuple), (5) velocity separation of pair (or velocity difference to closest galaxy in velocity within the n-tuple), (6) R absolute magnitude, extrapolated to the total magnitude and measured assuming $H_0 = 70 \text{ km s}^{-1} \text{ Mpc}^{-1}$, (7) color of the portion of the galaxy on the slit during the spectroscopic observation, corrected for Galactic extinction and nebular lines, (8) $H\alpha$ equivalent width, (9) Balmer decrement (corrected for Balmer absorption), (10) corrected velocity width, and (11) a description of rotation curve, where norm = “normal”, marg = “marginal” (intermediate between normal and distorted), and dist = “distorted” (see text of Barton et al. 2001), and (12) label for Figs. 23 and 24. [The complete version of this table will appear in the electronic edition of the Journal and is available from the first author.]

brightness profiles with ellipse fitting on the B -band images; we overlay B -band isophotes onto the R -band images. Barton et al. (2001) discuss the Galactic reddening correction and several issues relating to galaxy distortion and overlap.

BGK contains a complete description of the spectroscopy and data reduction. We observed the galaxies using the FAST spectrograph at the 1.5m Tillinghast telescope on Mt. Hopkins. Typical exposures lasted $\sim 10 - 20$ minutes. We observed the galaxies through a $3''$ slit using a grating with 300 lines/mm to disperse the light between 4000 and 7000 Å. The galaxies were often observed through clouds; thus, the spectra are roughly calibrated only in a relative sense, using observations of one or more spectrophotometric standards each night. The photometry of the galaxies provides a more reliable indicator of the overall continuum shape of the spectral energy distribution. Fig. 2 shows examples of the spectra, illustrating the observed range of star-forming properties.

After flatfielding the data, we extract apertures which include the brightest continuum light incident on the slit from the galaxy. This procedure results in a range of aperture lengths, from $0.25 - 13.7 \text{ h}^{-1} \text{ kpc}$, with a median of only $2.4 \text{ h}^{-1} \text{ kpc}$. Thus, strictly speaking, the spectra are not “nuclear” but “central” spectra encompassing the central light distribution. We compute equivalent widths that are the ratio of the flux in the line to the measured continuum. We base errors on photon statistics; repeat measurements indicate that these errors are within a factor of ~ 2 of the true measurement errors. We correct for Balmer absorption by computing the maximum absorption equivalent width in $H\delta$ or $H\gamma$ and adding that equivalent width to both $H\alpha$ and $H\beta$.

For the SP sample, we use the cleaned² 48-inch images (see Barton et al. 2001) to measure the B and R isophotal magnitudes, which we extrapolate to total magnitudes, and $B-R$ color, B_s , R_s , and $(B-R)_s$, respectively, of the light that accumulated through the slit during the spectroscopic observations. We compute these quantities by adding the flux within a rectangular aperture measuring $3'' \times L_{\text{ap}}$ and aligned with the spectroscopic aperture (to within $\lesssim 1.5^\circ$), for both the B and R clean images. $3''$ is the width of the slit and L_{ap} is the (variable) length of the

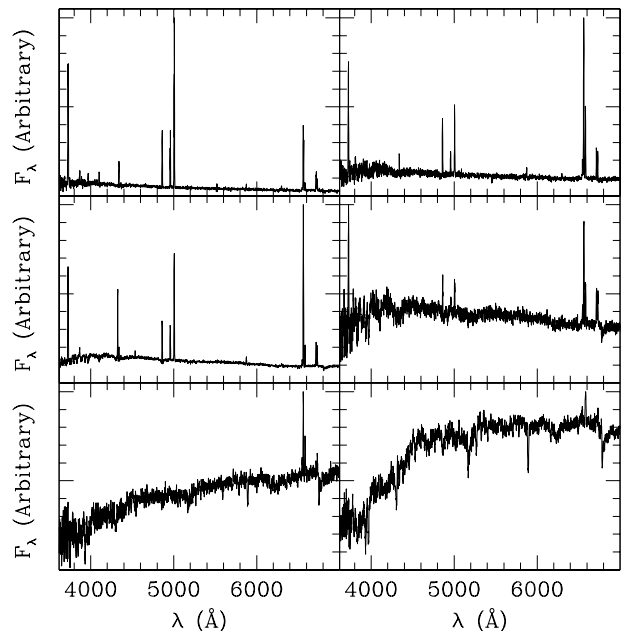


FIG. 2.— Sample spectra illustrating the range of observed star-forming properties of the interacting galaxies. To show the quality of the data, the spectra have not been smoothed.

extracted aperture. We assume the slit center and the center of the galaxy (the center of the smallest fit ellipse) are coincident, a close approximation to the actual position of the slit during the spectroscopic observation. We measure conservative errors in $(B-R)_s$ due to misplacement of the slit center by displacing the slit 2 pixels ($\sim 1.2''$) in the $\pm x$ and $\pm y$ directions, for a subset of 30 galaxies. Changes in the color range from ~ -0.1 to $\sim +0.2$ magnitudes, with $\sigma = 0.055$. When the spectrum consists of two or more exposures, usually with different values of L_{ap} , we scale the fluxes in the different apertures by the exposure times of the spectra; this procedure is only approximately correct in cases where the atmospheric absorption differed during

the observations.

Finally, we observed galaxies in the dynamical sample with the Blue Channel Spectrograph at the Multiple Mirror Telescope on Mt. Hopkins between November 1996 and February 1998. For the majority of the galaxies, we used a $1''$ slit and a grating with 1200 lines/mm centered at $\sim 6500 \text{ \AA}$, and including roughly the wavelength range $5800 - 7200 \text{ \AA}$.

Barton et al. (2000b) and Barton et al. (2001) describe the data reduction in detail. We use a cross-correlation technique that makes simultaneous use of the major emission lines: [NII] ($\lambda 6548$ and $\lambda 6583$), [SII] ($\lambda 6716$ and $\lambda 6730$), and $H\alpha$; this technique is straightforward to implement and yields well-defined errors. We use the method of Courteau (1997), developed for Tully-Fisher (Tully & Fisher 1977, TF hereafter) applications, to measure the velocity width, $V_{2,2}$, for galaxies in the dynamical sample. We fit each rotation curve with an empirical fitting function (see Courteau 1997, Eqn. 2). Barton et al. (2001) describe the corrections we apply for inclination, slit misalignment, and redshift, to arrive at $V_{2,2}^c$, the corrected velocity width.

3. PARAMETERIZING THE CENTRAL BURSTS OF STAR FORMATION

For lack of adequate constraints, full modeling of an unresolved stellar population requires assumptions about the star formation rate as a function of time. Many studies parameterize the star formation rate with a single function, such as an exponential, and fit for the timescale, τ (e.g., Larson & Tinsley 1978; Abraham et al. 1996; Bell & de Jong 2000); others find the best-fit spectral energy distribution from a set of empirical templates (e.g., Thompson, Weymann, & Storrie-Lombardi 2001). Because our goal is to parameterize a recent ($\lesssim 1$ Gyr) burst of star formation superposed on an otherwise typical galaxy, we must parameterize the “old” (pre-existing) and “new” (interaction-related) populations separately.

Several existing studies address this “added-burst” problem (e.g., Larson & Tinsley 1978; Kennicutt et al. 1987; Kennicutt, Tamblyn, & Congdon 1994). For all of these studies, there is a degeneracy associated with separating the new burst from the pre-existing galaxy: is the galaxy blue because its star formation rate has been constant or increasing with time throughout its history, or is it blue because of a strong triggered burst? Or, cast in terms of the pair population as a whole, does the range of colors observed in pairs result from the range of colors in the progenitor galaxies or from triggered bursts of star formation? One approach involves beginning with the distribution of colors vs. $EW(H\alpha)$ observed in the field and exploring the effects of short bursts of star formation (e.g., Kennicutt et al. 1987). However, every point in the color/ $EW(H\alpha)$ plane is reachable from a range of starting points. In an approach similar to the models of Larson & Tinsley (1978), we essentially fix assumptions about the pre-existing stellar populations and characterize bursts of star formation in terms of burst age and “strength”, testing the effects of modifying the initial assumptions. We avoid assumptions about mass-to-light ratios by defining burst strength in terms of the fraction of the R -band flux originating from the new burst. In Secs. 3.2-4 we discuss the full range of possibilities; we include a discussion of techniques for resolving the degeneracy between young pre-existing stellar popula-

tions and triggered bursts. We also discuss the effects of other properties, like metallicity, on our results. We demonstrate the effectiveness of using only $B-R$ and $EW(H\alpha)$ in Sec. 3.3.

3.1. The Two-Population Model

For simplicity, we begin by assuming that two distinct stellar populations contribute to the flux incident on the slit aperture during the spectroscopic observation: (1) a new population, solely responsible for any $H\alpha$ emission, which we denote by the subscript n , with B and R fluxes, $f_{Bn}(t)$ and $f_{Rn}(t)$, respectively, that turn on at $t=0$ and evolve as the burst ages, and (2) a pre-existing, older population, denoted by the subscript 0 , with fluxes f_{B0} and f_{R0} , which do not evolve significantly on the burst timescales ($\lesssim 1$ Gyr). We explore the effects of $H\alpha$ emission from the pre-existing stellar population in Sec. 3.2. With these assumptions, the $H\alpha$ equivalent width from spectroscopic measurements [$EW(H\alpha)_{\text{meas}}(t)$], slit B and R fluxes from calibrated photometry, and starburst models for simple burst histories, we estimate both the strengths and ages of the starbursts.

The old population increases the continuum around $H\alpha$. Therefore, the fractional strength of the (new) burst in R , $s_R(t) \equiv \frac{f_{Rn}(t)}{f_{R0} + f_{Rn}(t)}$, governs the relationship between $EW(H\alpha)_{\text{meas}}(t)$ and the $H\alpha$ equivalent width of the burst alone, $EW(H\alpha)_{\text{burst}}(t)$. The measured equivalent width is

$$EW(H\alpha)_{\text{meas}}(t) = s_R(t) \times k(z, SED_0, SED_b) \times EW(H\alpha)_{\text{burst}}(t), \quad (1)$$

where $k(z, SED_0, SED_b)$ is a factor of order unity ($0.9 \lesssim k(z, SED_0, SED_b) \lesssim 1.4$) that corrects for the difference between the burst strength in R and the burst strength at the continuum near $H\alpha$. $k(z, SED_0, SED_b)$ depends on the spectral energy distributions of the old stellar population (SED_0) and the burst (SED_b). We estimate $k(z, SED_0, SED_b)$ at the appropriate redshift for a given old stellar population and burst by using Bruzual & Charlot (1996) Salpeter τ -model spectral energy distributions for the old population, matched in $B-R$ to the nearest τ model at 14 Gyr from formation (with τ equal to an integral number of Gyr in most cases). We interpolate the Leitherer et al. (1999) burst model spectral energy distributions for the burst SED computed at a limited set of burst ages. We use the R filter function of Bessell (1990) and the B filter function of Buser & Kurucz (1978). In effect, we parameterize the old stellar population completely via $(B-R)_0$ which is an input parameter, and $k(z, SED_0, SED_b)$, which we compute from the Bruzual & Charlot (1996) models based on the input $(B-R)_0$.

The metallicity of the old stellar population has little effect on $k(z, SED_0, SED_b)$. For a fixed $(B-R)_0 = 1.5$, we estimate the effects of metallicity by computing $k(z, SED_0, SED_b)$ over the full range of strengths from 0 to 1 and the full range of ages, IMFs, metallicities, and star formation histories of the L99 models. The maximum difference in $k(z, SED_0, SED_b)$ introduced by assuming a non-solar metallicity (of either $0.4 Z_\odot$ or $2.5 Z_\odot$) is $< 1\%$. Hereafter, we use $Z = Z_\odot$ to compute $k(z, SED_0, SED_b)$.

The strength of the new burst also depends on the colors of the old and new stellar populations. The composite (measured) R -to- B flux ratio is

$$C_s(t) = \frac{C_0}{1 + s_R(t) \frac{|C_0 - C_n(t)|}{C_n(t)}}, \quad (2)$$

where C_0 and $C_n(t)$ are the R -to- B flux ratios of the light incident on the slit from the old and new populations respectively. The R -to- B flux ratios are related to the colors: $C_0 =$

² The “cleaned” images have been stripped of overlapping stars and, in some cases, overlapping companion galaxies; we usually replace the stripped regions with an elliptically symmetric model of the galaxy.

TABLE 2
 ASSUMPTIONS FOR BURST MODEL CONTOURS

Parameter	Assumption for Fig. 3	Other assumptions from this paper or BGK
Pre-existing population color, $(B-R)_0$	1.5	0.9 – 2.0 $1.5 + 0.75 \times [\log V_{2.2}^c - 2.5]$ $1.5 + 1.50 \times [\log V_{2.2}^c - 2.5]$ Peletier & Balcells (1996) bulges NFGS distributions
Burst IMF	“steep” ($\alpha = 3.3$)	“Salpeter” ($\alpha = 2.35$) “cutoff Salpeter” ($\alpha = 2.35$, Mass $< 30 M_\odot$)
Burst SFR(t)	Constant for 1 Gyr	Instantaneous
Burst metallicity	Solar	$0.4 Z_\odot, 2 Z_\odot$

$$\frac{f_{R0}}{f_{B0}} = 10^{(B-R)_0/2.5}, \quad C_s(t) = \left(\frac{f_{R0} + f_{Rn}(t)}{f_{B0} + f_{Bn}(t)} \right) = 10^{(B-R)_s/2.5}, \quad \text{and} \quad C_n(t) = \frac{f_{Rn}(t)}{f_{Bn}(t)} = 10^{(B-R)_n/2.5}.$$

The “strength” parameter in Eqns. 1 and 2, $s_R(t)$, is time-dependent. It represents the *current* fraction of the central R -band flux originating from the new burst; this fraction increases as the burst builds luminosity and decreases as the burst fades. We also consider a time-independent parameter, s_{100} , the flux at an age of 100 Myr [$s_{100} \equiv s_R(100\text{Myr})$]. Then at any other time,

$$s_R(t) = \frac{\frac{s_{100}}{1-s_{100}} 10^{0.4[M_R(100\text{ Myr}) - M_R(t)]}}{1 + \frac{s_{100}}{1-s_{100}} 10^{0.4[M_R(100\text{ Myr}) - M_R(t)]}}, \quad (3)$$

where $M_R(t)$ is the R -band absolute magnitude of the burst as a function of time.

3.1.1. Strengths and Ages from the Leitherer et al. Models

Starburst models predict the burst color, $(B-R)_n$, and the burst $H\alpha$ equivalent width, $\text{EW}(H\alpha)_{\text{burst}}(t)$, as a function of time. We use the Leitherer et al. (1999, L99 hereafter) starburst models for burst parameters. L99 model a starburst by “forming” stars according to an IMF with $\frac{dN}{dM} = CM^{-\alpha}$, where M is the stellar mass, α is the slope of the IMF, and C is a constant. With models from the literature or their own models for stellar evolution, stellar atmospheres, and nebular emission, they compute $\text{EW}(H\alpha)$ as a function of time for both the “instantaneous” starburst case, with a timescale $\tau \lesssim 10^6$ years, and the continuous case, with star formation over 10^9 years.

The L99 models have a range of metallicities ($0.05 Z_\odot, 0.2 Z_\odot, 0.4 Z_\odot, Z_\odot, 2Z_\odot$), and a range of IMFs, including an approximate Salpeter (1955) IMF, with $\alpha = 2.35$, from $1 - 100 M_\odot$, a Salpeter IMF with a $30 M_\odot$ high-mass cutoff, and a steeper function with $\alpha = 3.3$ from $1 - 100 M_\odot$ patterned after the high-mass segment of the Miller & Scalzo (1979) IMF. Hereafter, we refer to these IMFs as Salpeter, cutoff Salpeter, and steep, respectively.

For an assumed pre-existing stellar population, the starburst models and Eqns. 1 – 3 provide a method of estimating burst strengths, $s_R(t)$ or s_{100} , and ages, t , from the measured quantities $[(B-R)_s]$ and $\text{EW}(H\alpha)_{\text{meas}}(t)$. Fig. 3 shows contours of constant current burst strength, $s_R(t)$, and age, t , in the (measured) $\text{EW}(H\alpha)/(B-R)_s$ plane for a continuous burst of star formation with the “steep” IMF and $(B-R)_0 = 1.5$. Hereafter, we assume $cz = 5000 \text{ km s}^{-1}$ to compute $k(z, \text{SED}_0, \text{SED}_b)$, except for spe-

cific galaxies, for which we use the measured redshift. Table 2 summarizes the other assumptions we make to construct these contours. For comparison, Fig. 4 shows the contours of constant (current) burst strength assuming old population colors of $(B-R)_0 = 1.0$ and $(B-R)_0 = 2.0$.

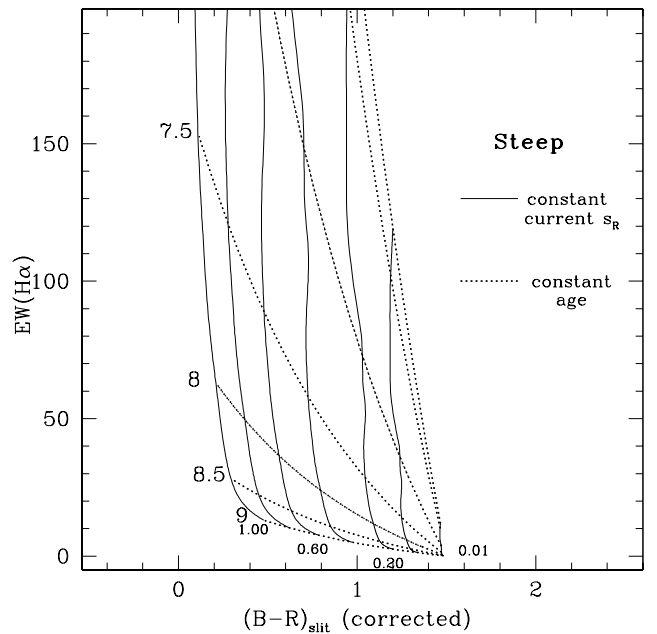


FIG. 3.— Contours of constant current burst strength and age in the plane of the observed parameters, for a continuous burst of star formation (see Table 2). The dotted lines are lines of constant burst age, t , in $\log(\text{years})$; solid lines are contours of constant *current* strength, $s_R(t)$, defined as the fraction of R -band flux from the new burst in the spectroscopic aperture.

Lines of constant t_{burst} are diagonal in Figs. 3 and 4, while the contours of constant $s_R(t)$ are nearly vertical. Thus, for continuous bursts of star formation with steep IMFs superposed on fixed existing stellar populations, the burst age, t_{burst} , primarily affects the measured $\text{EW}(H\alpha)$. In contrast, the strength of the burst in R , $s_R(t)$, affects both the measured $\text{EW}(H\alpha)$ and the measured color, $(B-R)_s$.

Contours of constant s_{100} in Fig. 5 are the evolutionary tracks of constant bursts of star formation within this model. s_{100} is

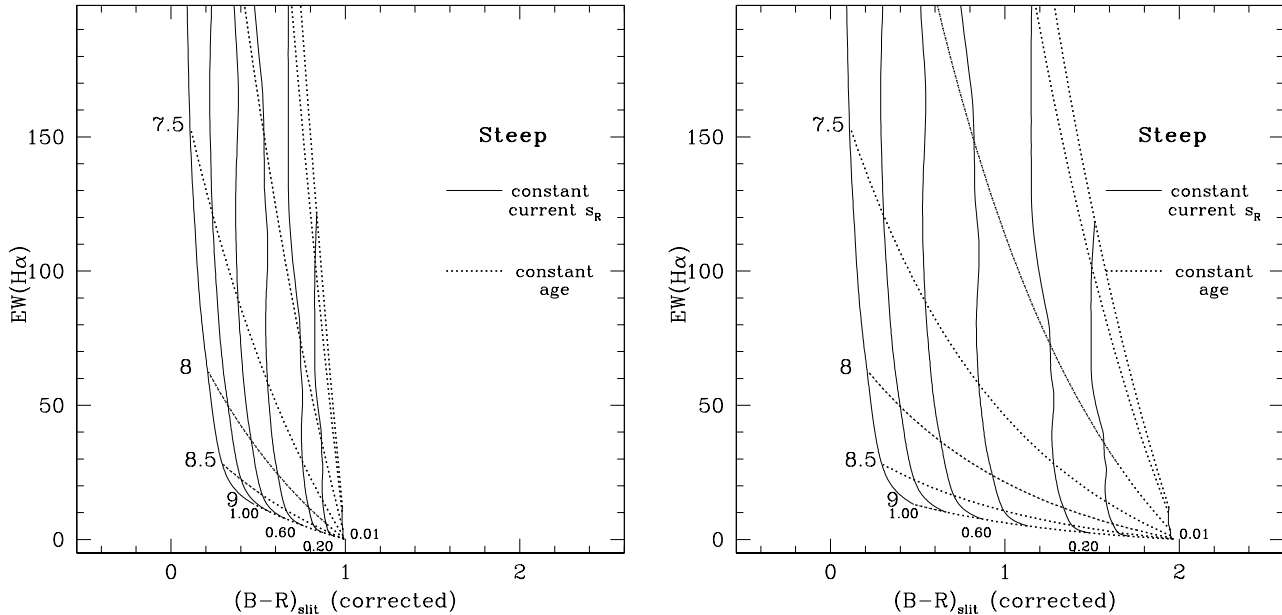


FIG. 4.— Same as Fig. 3, but with $(B-R)_0 = 1.0$ (left) and $(B-R)_0 = 2.0$ (right). Lines of constant current strength, $s_R(t)$, remain roughly vertical, but the lines corresponding to weaker bursts are displaced depending on $(B-R)_0$. The blue edge of the contours is independent of $(B-R)_0$; the IMF and the starburst models determine the location of a population that is 100% triggered burst.

the burst strength in R that would be measured at 100 Myr, assuming that the burst continues (or has continued) at a constant rate. s_{100} depends heavily the assumption of a constant star formation rate. Mass-fraction measures (e.g., Larson & Tinsley 1978; Kennicutt et al. 1987) require similar assumptions; they incorporate assumptions about the relative mass-to-light ratios of the burst and the underlying old stellar population.

The contours in Fig. 5 fold over and are no longer vertical. A moderately strong, young burst continuing at its current rate dominates the flux of the galaxy at 100 Myr. For example, within this model, if a continuous burst superposed on an older population [$(B-R)_0 = 1.5$] has $EW(H\alpha)_{\text{meas}}(t) = 120 \text{ \AA}$ and $(B-R)_s = 0.6$, its current age (Fig. 3) is ~ 16 Myr and $\sim 50\%$ of the R -band flux currently originates from this burst. If this burst continues at its present rate, at 100 Myr it will comprise $\sim 80\%$ of the R -band flux in the aperture (Fig. 5). If the burst actually ceases at 316 Myr, it will comprise much less than the original 50% of the R -band flux in the aperture at 100 Myr.

3.2. Measuring Strengths and Ages from the Data

The discussion in Sec. 3.1.1 omits several corrections necessary to apply the models to the data. Table 3 summarizes the corrections we discuss in this section. They include (1) the contribution from line emission to $(B-R)_s$, which we estimate using the measured equivalent widths of the nebular lines along with the continuum from the model spectral energy distributions. We apply the nebular emission (and absorption) corrections to the color data in the slit regions only (not to the total magnitudes), and include the corrections in Figs. 3 – 5; the corrections range from -0.079 to 0.003 with an average of -0.017 , (2) extinction corrections to the measured colors and/or $EW(H\alpha)_{\text{meas}}(t)$, and (3) ongoing star formation in the pre-existing stellar population. Finally, we discuss our choices for the color of the pre-existing stellar population, $(B-R)_0$.

TABLE 3
CORRECTIONS TO THE DATA

Correction	Correction(s) explored in this paper
nebular line contamination in color	corrected data using measured equivalent widths, model SEDs
Internal reddening	“traditional” ^a none “Calzetti” ^b
ongoing star formation in pre-existing stellar population	no correction applied

^aSee Sec. 3.1.

^bCalzetti, Kinney, & Storchi-Bergmann (1994); see Sec. 3.1.

3.2.1. Corrections for Extinction

Corrections for internal extinction substantially modify the inferred ages and strengths of the bursts of star formation. Because it is independent of the star formation history of the galaxy, the Balmer decrement³ is generally the best extinction measure available in our dataset. However, several circumstances affect our ability to measure the Balmer decrement and to derive the appropriate extinction correction for the galaxy. The presence of an intermediate-age (\sim Gyr) population necessitates a correction for Balmer absorption under the emission lines (see Sec. 2.1 and BGK for a description of our correction). In addition, Calzetti, Kinney, & Storchi-Bergmann (1994) show that the extinction of the continuum is only half of that appro-

appropriate for line-emitting regions.

The difficulty of measuring the Balmer decrement in galaxies with insufficient star formation introduces selection effects into the extinction-corrected sample. The top panel of Fig. 6 shows the fractional error in the Balmer decrement as a function of $\text{EW}(\text{H}\alpha)$ for the 78 galaxies with accurate measurements (better than 25%); 112/190 galaxies yield larger errors in $\text{H}\alpha/\text{H}\beta$ or exhibit no significant $\text{H}\beta$ emission. The bottom panel shows a histogram of $\text{EW}(\text{H}\alpha)_{\text{meas}}(t)$ for the galaxies with no $\text{H}\alpha/\text{H}\beta$ measurements; incompleteness in the sample of galaxies with accurate Balmer decrement measurements begins at $\text{EW}(\text{H}\alpha)_{\text{meas}}(t) \sim 20 \text{ \AA}$. In the analysis below, we primarily use the 78 galaxies with accurate measures; we replace values of $\text{H}\alpha/\text{H}\beta < 2.85$ with 2.85 (or 2.88 as necessary).

We explore the possible effects of dust on our data by considering three different dust corrections: no correction, a “traditional” correction with no differences in extinction between the continuum and the line-emitting regions, and the extinction correction of Calzetti, Kinney, & Storchi-Bergmann (1994, “Calzetti” correction, hereafter).

The “traditional” correction involves no adjustments to $\text{EW}(\text{H}\alpha)_{\text{meas}}(t)$. We correct $(B-R)_s$ for reddening assuming

$$\begin{aligned} E(B-R) &= 1.78E(B-V) = 1.536E(\beta-\alpha) \\ &\equiv 1.536 \times 2.5 \log \left[\frac{(\text{H}\alpha/\text{H}\beta)}{2.85} \right] \end{aligned}$$

(Zombeck 1990; Miller & Mathews 1972; Veilleux et al. 1995). Here, $E(B-R)$, $E(B-V)$, and $E(\beta-\alpha)$ are the B -to- R , B -to- V , and $\text{H}\beta$ -to- $\text{H}\alpha$ reddening, respectively, and $\text{H}\alpha/\text{H}\beta$ is the flux ratio of $\text{H}\alpha$ to $\text{H}\beta$, corrected for Balmer absorption. The error in

³ The Balmer decrement is the flux ratio $\text{H}\alpha/\text{H}\beta$, where both fluxes have been corrected for stellar absorption with the prescription described in Barton, Geller, & Kenyon (2000a).

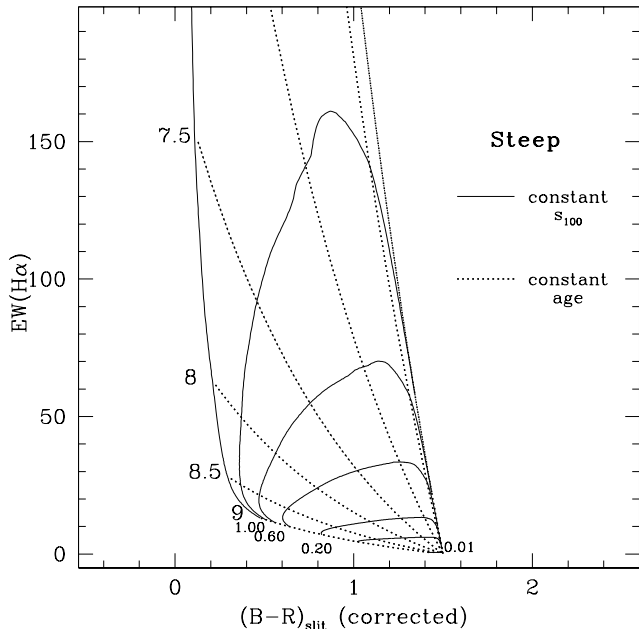


FIG. 5.— Same as Fig. 3, except that solid lines are contours of constant strength for the burst at 100 Myr. Thus, constant s_{100} lines track the evolution of a continuing burst of star formation. Unlike $s_R(t)$, the measurement of s_{100} depends heavily on the assumption the burst star formation rate is constant.

the measured $\text{H}\alpha/\text{H}\beta$ includes a small addition for uncertainty in the Balmer absorption correction.

The “Calzetti” correction is appropriate if dust is clumped around regions of recent star formation (e.g., Charlot & Fall 2000); the prescription requires separate corrections for the continuum and line emission (Calzetti, Kinney, & Storchi-Bergmann 1994):

$$E(B-R) = 0.8170 \ln \left[\frac{\text{H}\alpha/\text{H}\beta}{2.88} \right]$$

and

$$\text{EW}(\text{H}\alpha)^c = \text{EW}(\text{H}\alpha)_{\text{meas}}(t) \times \left[\frac{\text{H}\alpha/\text{H}\beta}{2.88} \right]^{0.9005}$$

3.2.2. Star Formation in the Pre-existing Stellar Population

In this section, we discuss our choice not to correct for ongoing star formation in the pre-existing stellar population. The appropriate corrections depend on the intended interpretation of the results. The fundamental question is whether the new burst of star formation is physically independent of the ongoing star formation in the progenitor galaxy. If the pre-existing stellar population and the recently-formed burst population are truly independent of one another, ongoing star formation in the pre-existing (“old”) population necessitates corrections to the data and models. Non-zero corrections to $\text{H}\alpha$ result in weaker burst strengths and older burst ages. We argue, however, that once an interaction disrupts a galaxy, star formation is not independent in the pre-existing and burst populations. The process that triggers the new, added burst of star formation likely disrupts the “quiescent” star formation in the galaxy. The triggered burst may consume the gas that was forming stars in the absence of an interaction, invalidating the assumption of physically independent pre-existing and burst populations.

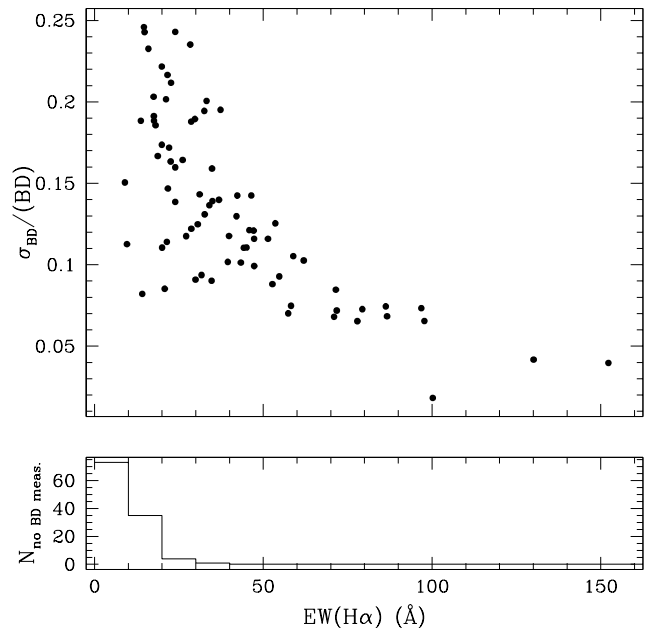


FIG. 6.— (Top) Fractional error in the Balmer decrement as a function of $\text{EW}(\text{H}\alpha)_{\text{meas}}(t)$. Our cutoff is an error of 25% of the measured value. (Bottom) Histogram of the galaxies with $> 25\%$ errors. The set of galaxies with measured Balmer decrements is incomplete for $\text{EW}(\text{H}\alpha)_{\text{meas}}(t) \lesssim 20\text{--}30 \text{ \AA}$.

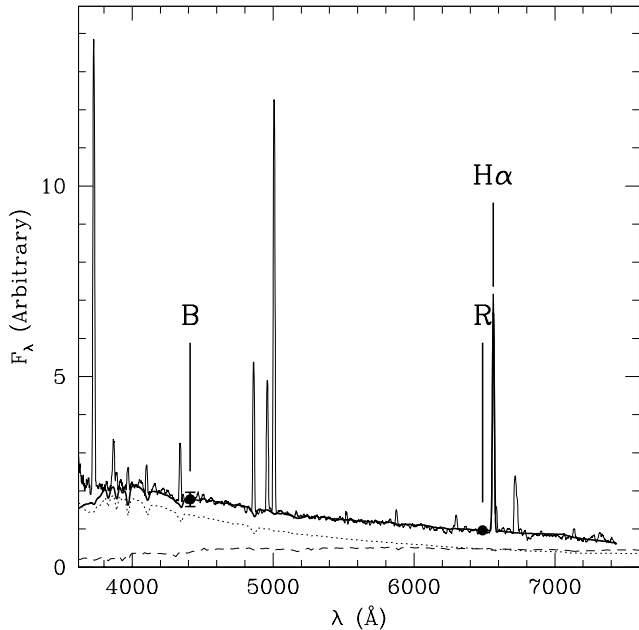


FIG. 7.— An example of the model spectrum and the galaxy spectral energy distribution for the “clean” case of NGC 2719A, which has a Balmer decrement consistent with no reddening. The thick black line is the spectral energy distribution of the model, fit to the $B-R$ color and $\text{EW}(\text{H}\alpha)$ of the center of the galaxy only. The model is the sum of the relevant L99 model, a 21-Gyr-old burst with a “steep” IMF, and the Bruzual & Charlot (1996) model with a Salpeter IMF and an exponential star formation timescale of $\tau = 3$ Gyr, observed 14 Gyr after formation. The other nebular emission lines are not modeled. We plot broad band fluxes as filled circles; R is normalized to the spectrum and B is plotted at its effective wavelength. The data and models have both been smoothed by 10 bins.

Without physical distinctions between the pre-existing and triggered populations, the amount of triggered star formation is an ill-defined quantity. Two better-defined, distinct quantities are: (1) the statistical increase in central star formation due to major interactions, and (2) the total star formation ongoing in the centers of interacting galaxies (including star formation that would have occurred in the absence of a major interaction). Measuring these quantities requires different approaches to the correction for ongoing star formation in the pre-existing stellar population. The first requires a statistical correction for quiescent star formation; the second question requires no correction, but a judicious choice for $(B-R)_0$ that allows for the possibility of star formation just prior to the interaction.

Regardless of the interpretation, a moderate amount of ongoing star formation in the pre-existing stellar population has few qualitative effects. The primary effect is to place galaxies with no interaction-triggered star formation onto the apparent burst contours (as in Fig. 3). These galaxies occupy a locus across the lower portion of the $(B-R)_s/\text{EW}(\text{H}\alpha)_{\text{meas}}(t)$ plane defined by “normal” galaxies. For these galaxies, the model analysis is not applicable. Thus, some of the galaxies that appear, in this model, to have weak bursts of star formation may actually be quiescent late-type galaxies; our analysis is more reliable for galaxies with larger $\text{EW}(\text{H}\alpha)_{\text{meas}}(t)$.

In the sections that follow, we focus on the approach of characterizing the physical conditions in galaxies with triggered star formation. We apply no corrections for ongoing star-formation directly to the data, but explore the effects of different choices for $(B-R)_0$.

3.3. The Scope of the Model

To characterize the star-forming properties of our galaxies, our approach is to fit simple star-formation models to the observed $B-R$ colors and $\text{EW}(\text{H}\alpha)$ in the centers of the galaxies, using spectral synthesis models from the literature (Leitherer et al. 1999; Bruzual & Charlot 1996). These models predict the entire spectrum of the galaxy, with the exception of most of the nebular line strengths; the agreement between the predicted and observed spectra serves as a consistency check of our models. Fig. 7 shows the “clean” case of NGC 2719A, with a measured Balmer decrement that yields no evidence for reddening in the spectrum. The thin solid line is the data; the thick solid line is sum of the model spectra from Bruzual & Charlot (1996) and L99, respectively; we also include the $\text{H}\alpha$ line, with the appropriate measured $\text{EW}(\text{H}\alpha)$. For the old stellar population (*dashed line*), we use a $\tau = 3$ model with a Salpeter IMF at 14 Gyr, corresponding to $(B-R)_0 = 1.46$ [close to our fiducial $(B-R)_0 = 1.5$]. The measured $(B-R)_s = 0.56$ and $\text{EW}(\text{H}\alpha) = 100 \text{ \AA}$ yield a burst strength and age of 0.51 and 21.4 Myr, respectively, for this $(B-R)_0$ and the “steep” IMF, with solar metallicity. Hence, the “new burst” spectrum (*dotted line*) is the L99 model with continuous star formation and “steep” IMF after 21 Myr. The thick black line is the sum of these models, combined according to the derived value of $s_R(t)$. Filled circles represent measured $B-R$ color, plotted at the effective wavelength of each band with both filter passbands from Bessell (1990); we normalize R and plot B . By design, the broad-band color agrees perfectly with the model.

Apart from the nebular emission lines, which are not predicted by the models, the spectral shape agrees well with the model, even though it is not used as an input. This agreement results from the agreement between the rough calibration of the spectrum and the more reliable broad band colors, which are generally within ~ 0.2 magnitudes of one another for the galaxies with no reddening. The exception is the very blue end, below $\sim 4000 \text{ \AA}$, where the calibration of the spectrum is highly uncertain. The good agreement between the predicted spectrum and the observed spectrum justifies our use of only the broad band colors and $\text{EW}(\text{H}\alpha)$ *a posteriori*: the spectra do not contain any more of the information predicted by the model than we are already using. In particular, the model spectra corresponding to other $(B-R)_0$ values [and adjusted according to the new derived $s_R(t)$ and t_{burst}] appear to agree similarly well, within the limits of the expected accuracy of the calibration of the spectrum, indicating that the optical spectra contain no additional reliable information about the color of the pre-existing stellar population.

Broadly speaking, the spectral energy distribution of a galaxy with a triggered burst of star formation is determined by a large number of factors, including the metallicities, star formation histories, and IMFs of both the old and new stars, and the reddening appropriate for each stellar population. As indicated above, the current dataset does not provide separate information about all of these quantities. Our approach is to identify the most significant factors and focus on their effects. As we describe in Sec. 3.1, for the fiducial $(B-R)_0 = 1.5$, the metallicity of the old stellar population only affects $k(z, \text{SED}_0, \text{SED}_b)$ by $< 1\%$. In Sec. 3.4, we characterize the effects of the metallicity of the burst and show that they are dwarfed by uncertainties in the burst IMF and old stellar population color. Hence, we focus on the most important factors, the star formation histories, burst IMF, and reddening corrections. Our approach, as

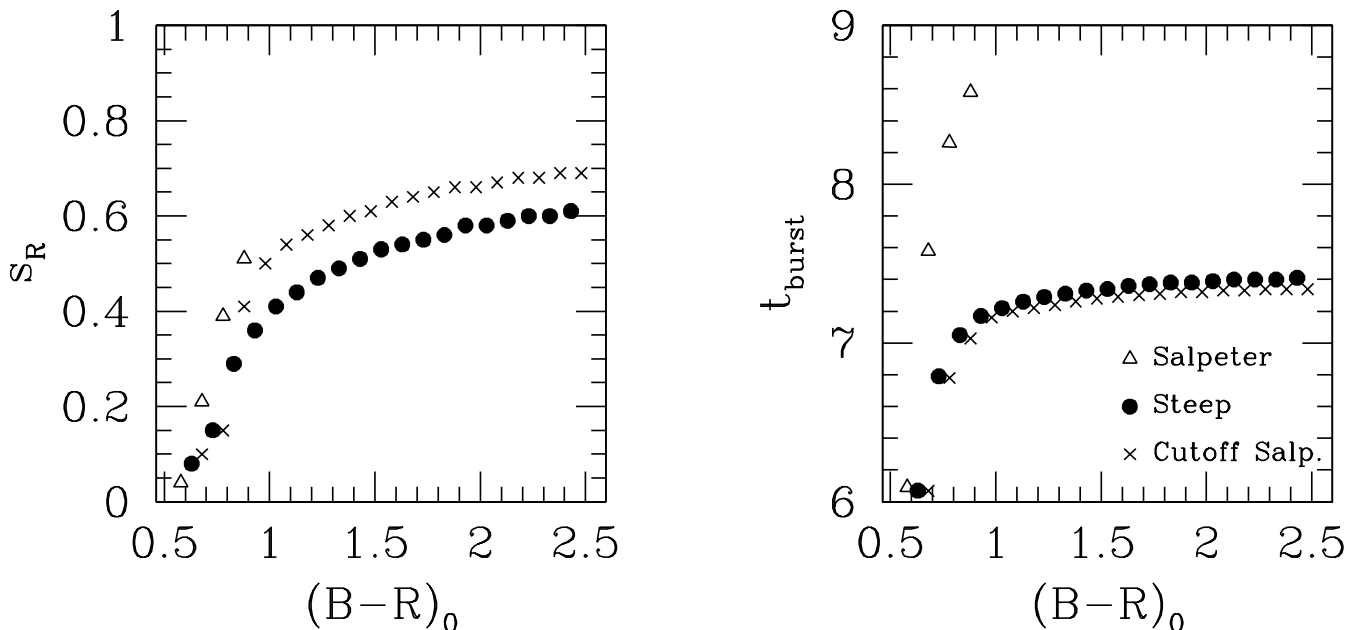


FIG. 8.— Solutions for burst strength, $s_R(t)$ (left), and age, t_{burst} (right) for NGC 2719A as a function of $(B-R)_0$, for the three different IMFs, assuming solar metallicity. NGC 2719A has $\text{EW}(\text{H}\alpha) = 100 \text{ \AA}$ and $(B-R)_s = 0.56$ with no evidence for extinction in the optical spectrum.

described above, is to parameterize the burst star formation history in terms of an age, t_{burst} , and a current R -band strength, $s_R(t)$, and compute the results for a set of different assumptions about the burst IMF, the reddening, and the old stellar population star formation history and IMF [as characterized together by $(B-R)_0$]. Our argument is statistical in nature; we attempt to account for the relationship between the ensemble properties of the sample and the predictions of the models.

3.4. Results

The measured $s_R(t)$ and t_{burst} depend relatively strongly on the input color of the old stellar population, $(B-R)_0$. Fig. 8 shows this dependence for NGC 2719A, the galaxy depicted in Fig. 7 with a strong burst of star formation and no apparent reddening. The realistic possibilities for $(B-R)_0$ do not include the entire range in the figure (from 0.5 – 2.5). For galaxies of types S0 to Sbc, Peletier & Balcells (1996) find bulge colors in the range of $1.15 \leq B-R \leq 1.8$; centers of later-type spirals and irregulars are as blue as ~ 0.8 for “field” galaxies (Bell & de Jong 2000).

The uncertainties in the assumptions about IMF and $(B-R)_0$ dwarf the uncertainties introduced by assuming solar metallicity for the old and new bursts. As discussed in Secs. 3.1 and 3.3, uncertainties introduced by the metallicity of the old stellar population are negligible. Fig. 9 illustrates the typical effects of our assumption of solar metallicity for the burst; the effects are small compared with the other uncertainties. To verify that the observed range of metallicities in our sample is limited, we use the “combined” metallicity estimator of Kewley & Dopita (2002); 99/190 of the SP sample spectra exhibit strong enough emission lines to make this measurement. For a solar abundance of $\log(O/H) + 12 = 8.69$ (Allende Prieto, Lam-

bert, & Asplund 2001), the metallicities range from $0.42 Z_\odot$ to $4.01 Z_\odot$ with a median of $1.69 Z_\odot$. For the galaxies with measured Balmer decrements, 4 have metallicities closer to the L99 model with $Z = 0.4Z_\odot$ and 47 have metallicities closer to the model with $Z = 2Z_\odot$. We test the differences between using the solar metallicity model and the model closer in metallicity. Assuming $(B-R)_0 = 1.5$, the *maximum* differences in $s_R(t)$ and t_{burst} are 0.06 and 15.9 Myr, respectively. Thus, we assume solar metallicity hereafter, which has no qualitative effects on our conclusions.

Our data are insufficient to distinguish among different values of $(B-R)_0$. However, optical-to-near-infrared colors will aid in the process. For example, a galaxy like NGC 2719A, with measured $\text{EW}(\text{H}\alpha) = 100 \text{ \AA}$ and $(B-R)_s = 0.56$ has equally valid solutions for steep-IMF bursts of (among others) $s_R(t) = 0.54$ and $t_{\text{burst}} = 23 \text{ Myr}$ if $(B-R)_0 = 1.64$ and $s_R(t) = 0.3$, $t_{\text{burst}} = 12 \text{ Myr}$ if $(B-R)_0 = 0.86$. With a Salpeter-IMF burst on the same pre-existing blue galaxy, the solution differs even more significantly in age, with $t_{\text{burst}} = 329 \text{ Myr}$ and $s_R(t) = 0.48$. Using Bruzual & Charlot (1996) Salpeter IMF τ models for the pre-existing galaxies, with $\tau = 1 \text{ Gyr}$ and $\tau = 100 \text{ Gyr}$ (i.e., a constant star formation rate), respectively, we predict differences in the burst+pre-existing galaxy $V-K$ colors of 0.17 magnitudes between the two solutions with steep IMFs, and 0.29 magnitudes between the steep IMF solution on the red pre-existing population and the Salpeter-IMF solution on the blue pre-existing population, with the redder $V-H$ colors for the $\tau = 1 \text{ Gyr}$ Salpeter pre-existing population model and the steep-IMF burst. Thus, near-infrared colors help to distinguish among star formation histories and IMFs.

Without near-infrared data, we must make assumptions about the properties of the pre-existing stellar populations. Fig. 10

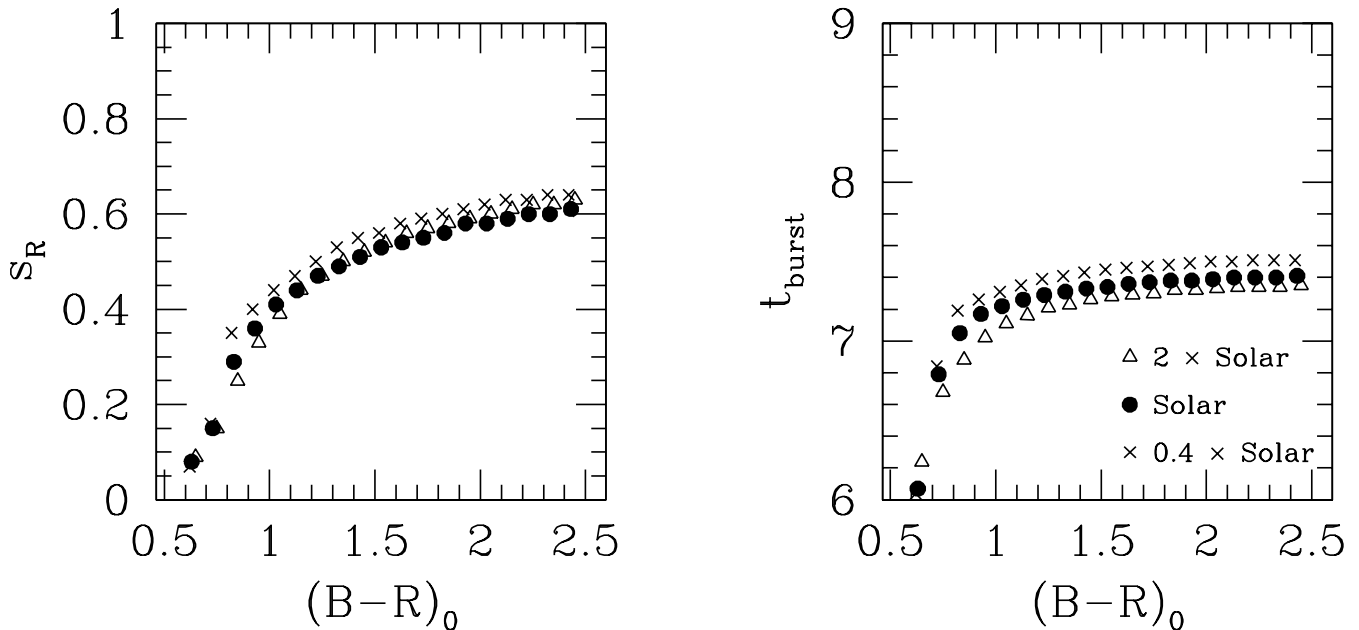


FIG. 9.— Solutions for burst strength, $s_R(t)$ (left), and age, t_{burst} (right) for NGC 2719A, as a function of $(B-R)_0$, for models with three different burst metallicities and a “steep” IMF. Comparison with Fig. 8 indicates that the uncertainties in the assumptions about IMF and old stellar population color dominate over the effects of assumptions about metallicity.

shows the range of central-aperture colors in our sample. We segregate the sample into galaxies with substantial ongoing star formation (*left*, $\text{EW}(\text{H}\alpha) > 10 \text{ \AA}$) and galaxies with little ongoing star formation (*right*, $\text{EW}(\text{H}\alpha) < 10 \text{ \AA}$). We expect some contributions from triggered star formation even to the right side of the figure because timescales for blue $B-R$ colors are substantially longer than timescales for $\text{H}\alpha$ emission. Despite the contribution from triggered bursts, the outer edge of the distribution (from interlopers and/or galaxies with no triggered star formation) provides an upper limit to the appropriate value of $(B-R)_0$. For illustrative purposes, we choose a fiducial constant value $(B-R)_0 = 1.5$ (vertical line in Fig. 10b).

Fig. 11 shows the 78 pair galaxies with measurable Balmer decrements (hence relatively strong ongoing star formation) on the continuous star formation model contours with $(B-R)_0 = 1.5$ for three IMFs and three reddening corrections. The points fall in the expected range for the steep and cutoff Salpeter IMF slopes, based on all but the “traditional” reddening correction, which over-corrects continuum colors. For comparison, Fig. 12 shows the contours and data with $(B-R)_0 = 0.9$.

Although the absolute positions of the points on the contours are extremely uncertain, for a given $(B-R)_0$ the relative positions of the galaxies in the $(B-R)_s/\text{EW}(\text{H}\alpha)_{\text{meas}}(t)$ plane are more reliable. To the extent that a constant $(B-R)_0$ is valid, one conclusion from Fig. 11 is that the galaxies in our sample with larger $\text{EW}(\text{H}\alpha)_{\text{meas}}(t)$ have stronger and younger bursts of star formation. The more complex models that follow confirm this interpretation.

3.4.1. Constraints on the IMF

For all reddening corrections, most of the data fail to overlap the Salpeter model contours in Figs. 11 and 12. Most of the data that are bluer than the assumed $(B-R)_0$ fall below the constant- $(B-R)_0$ Salpeter contours, corresponding to ages $\gg 10^9$ years. Timing arguments alone rule out this possibility for the majority of the data; thus, if the Salpeter slope is correct, one or more of the other assumptions are invalid. Different *constant* (galaxy-independent) $(B-R)_0$ values do not affect the results; changes in $(B-R)_0$ only shift contours horizontally. Different star formation histories also fail to solve the problem convincingly. Replacing the continuous star formation models with short (or instantaneous) bursts yields ages of $\ll 10^7$ years for all of the bursts. Although our data do not strictly rule out the instantaneous-burst scenario, interaction timescales are $\gtrsim 300$ Myr, or ~ 50 times the duration of this burst; only a tiny fraction of our sample would then be bursting. This argument does not rule out bursty star formation occurring *quasi-continuously*. In a time-averaged sense, a bursty star formation history mimics a steeper IMF — in the time between bursts, the highest-mass stars are preferentially removed. Thus, our data do not strictly distinguish between a steeper IMF and a shallower IMF with bursty star formation.

For simpler (non-bursty) star formation histories, our models and observations suggest either (1) a burst IMF with a high-mass slope steeper than the Salpeter IMF or, (2) bursts of star formation with a Salpeter-type IMF that produce smaller changes in the galaxy color. In other words, for Salpeter-IMF bursts to work, hence to lie on contours like those in Figs. 11 and 12, the $(B-R)_0$ color must shift with each galaxy — its color must be determined not by the burst but primarily by the

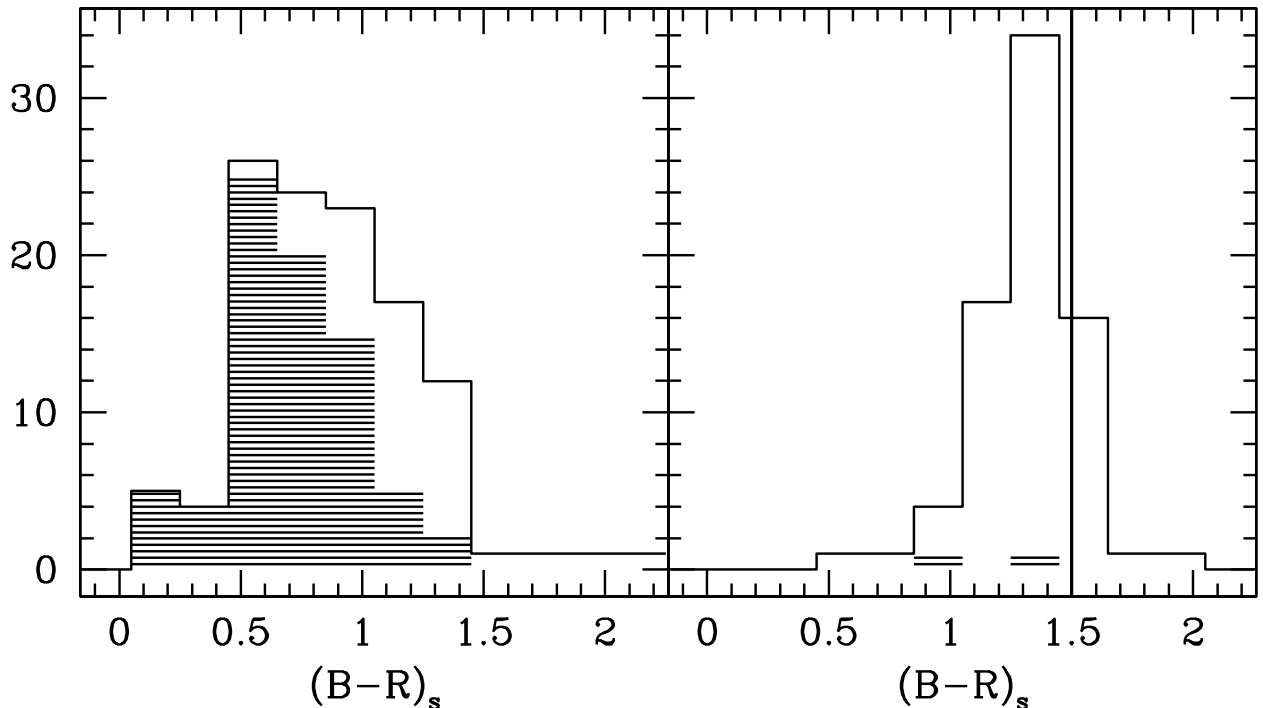


FIG. 10.— $(B-R)_s$, corrected for reddening and nebular lines with the “Calzetti” prescription, for: (a) line-emitting galaxies, with $\text{EW}(\text{H}\alpha) > 10 \text{ \AA}$, and (b) galaxies with $\text{EW}(\text{H}\alpha) < 10 \text{ \AA}$. The vertical line shows our choice of $(B-R)_0 = 1.5$.

pre-existing galaxy.

Near-infrared colors will help to distinguish between these possibilities in the future. In addition, a different line of argument, available to us now, results from the anti-correlation reported in BGK between $\text{EW}(\text{H}\alpha)$ and pair separation on the sky, ΔD . In the next section, we adopt different distributions of $(B-R)_0$ from the literature and investigate the relationship between the burst IMFs and the possible origins of the $\Delta D - \text{EW}(\text{H}\alpha)$ correlation.

4. THE ORIGINS OF THE $\Delta D - (B-R)_s - \text{EW}(\text{H}\alpha)$ DISTRIBUTION

The primary result of the spectroscopic study of BGK is the dependence of $\text{EW}(\text{H}\alpha)$ and the other emission lines on the pair separation on the sky, ΔD . The equivalent widths also correlate with velocity separation, ΔV . BGK find that galaxies in pairs with smaller spatial separations have a much larger range of $\text{EW}(\text{H}\alpha)$, whereas galaxies with larger separations (up to $\sim 50 \text{ h}^{-1} \text{ kpc}$) almost always have equivalent widths $\lesssim 30 \text{ \AA}$. BGK show that the correlation can be explained by a scenario in which a burst of star formation begins at a close pass, continuing and aging as the galaxies move apart. In this picture, the dynamical timescales match star formation timescales (for the steep IMF). The picture is also broadly consistent with the hydrodynamical simulations of Mihos & Hernquist (1996); Tissera et al. (2002) for progenitor galaxies with shallow central potentials (no bulges). The biggest uncertainty in the BGK picture is the contribution to $\text{EW}(\text{H}\alpha)$ from reddening and from old stellar populations in the centers of the galaxies. Our analysis of B and R photometry provides new constraints on this problem.

Fig. 13 shows the steep IMF model $(B-R)_0 = 1.5$ contours

along with our data corrected according to the “Calzetti” reddening law and segregated based on ΔD . We show only galaxies with $\Delta D < 20 \text{ h}^{-1} \text{ kpc}$ (filled circles) or $\Delta D > 30 \text{ h}^{-1} \text{ kpc}$ (open circles). Although the results depend on the IMF and the reddening correction, the plot suggests that for the single- $(B-R)_0$ model, the bursts in the galaxies with small separations and large $\text{EW}(\text{H}\alpha)$ are typically both younger *and* stronger than the bursts in the other galaxies, including the galaxies with larger separations on the sky. For a constant burst strength [$s_{\text{R}}(t)$ or s_{100}], the galaxies in pairs with smaller ΔD tend to have younger bursts.

In Sec. 3.4, we show that our model fails for Salpeter-IMF bursts if the progenitor galaxies have a very narrow $(B-R)_0$ range; the Salpeter model contours do not occupy the appropriate region in $(B-R)_s - \text{EW}(\text{H}\alpha)$ space. These arguments do not, however, rule out Salpeter bursts superposed on galaxies with a wide range of $(B-R)_0$. Here, we construct a simple Monte Carlo simulation to test whether Salpeter- or steep-IMF bursts and correlations between ΔD and $s_{\text{R}}(t)$ and/or ΔD and t_{burst} can give rise to the appropriate observed ranges of $\text{EW}(\text{H}\alpha)$ and $(B-R)_s$ and to the observed $\Delta D - \text{EW}(\text{H}\alpha)$ correlation [and relative lack of $\Delta D - (B-R)_s$ correlation]. We restrict the comparison to the 72 galaxies with $\text{EW}(\text{H}\alpha) > 15 \text{ \AA}$ and measured Balmer decrements, also applying this $\text{EW}(\text{H}\alpha)$ limit to the simulated data.

For the simulation, we draw 72 values of $(B-R)_0$ from the bulge colors of Peletier & Balcells (1996). We then draw a value of ΔD from a uniform distribution as indicated by the data; this uniform distribution represents an excess of very tight pairs over a random spatial distribution. For each tested maximum burst age and strength, t_{max} and $s_{\text{R,max}}$, respectively, we explore the effects of correlations between pair separation, ΔD ,

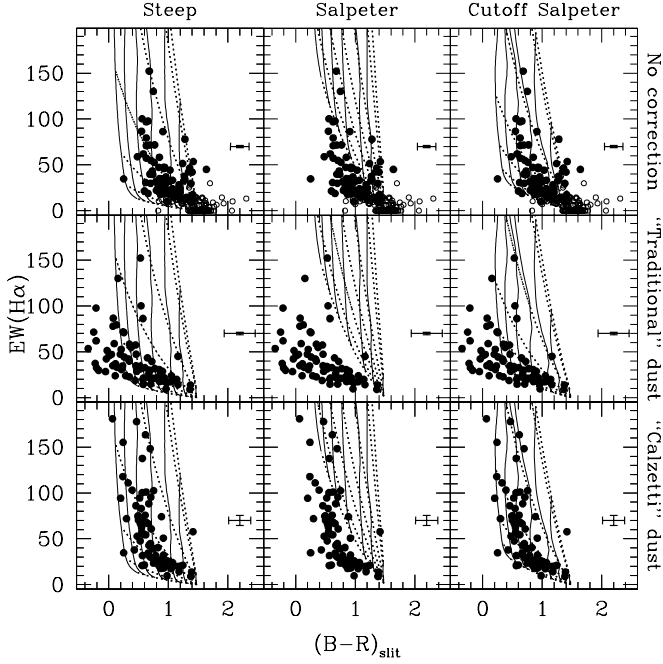


FIG. 11.— Pair data and model contours of constant $s_R(t)$ and t (see Fig. 3). Our model assumptions are described in Table 2, except we vary the IMF in the three columns: (left column) L99 steep IMF, (middle column) L99 Salpeter IMF, and (right column) L99 Cutoff Salpeter IMF. We correct the data for extinction according to three prescriptions for dust (see Sec. 3.2.1): (top row) no correction (except for Galactic extinction), (middle row) “traditional” correction, and (bottom row) “Calzetti” correction. We omit contour labels; they are the same as Fig. 3: (solid, left to right) $s_R(t) = 1, 0.8, 0.6, 0.4, 0.2, 0.01$ and (dotted, bottom to top) $t = 10^9, 10^{8.5}, 10^8, 10^{7.5}, 10^7, 10^{6.5},$ and 10^6 years. The lines on the right side of the plot show the median errors for the galaxies with measured Balmer decrements. For dust-corrected points, errors include propagated errors in the Balmer decrement. We plot the 112 galaxies with no measured Balmer decrement on the top line only (open circles).

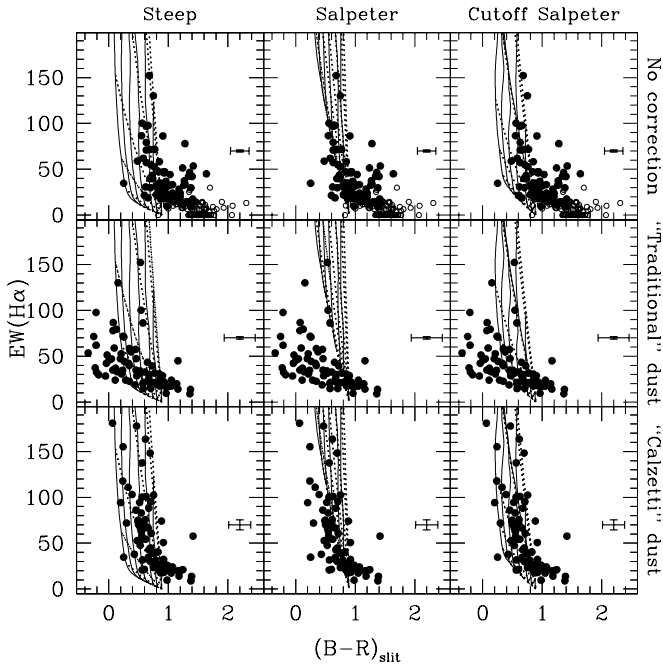


FIG. 12.— Same as Fig. 11 except $(B-R)_0 = 0.9$.

and $s_R(t)$ and/or t_{burst} . We test correlations that are “envelopes”, appropriate because ΔD is only a constraint on the minimum

physical separation of the pair (or compact group). For a given ΔD , we draw $s_R(t)$ from 0 to $s_{R,\text{max}} \times \left[1 - c_s \frac{\Delta D}{(50 \text{ kpc})}\right]$. This procedure results in a range of $s_R(t)$ values from 0 to $s_{R,\text{max}}$, with the maximum possible only at $\Delta D = 0$ for nonzero c_s . Similarly, we draw t_{burst} from $t_{\text{max}} - (t_{\text{max}} - 6 \text{ Myr}) \times \left[1 - c_t \frac{\Delta D}{(50 \text{ kpc})}\right]$ to t_{max} , resulting in a range of t_{burst} values from 6 Myr to t_{max} Myr, with the minimum possible only at $\Delta D = 0$. The parameters c_s and c_t are the slopes of the “envelopes” and measure the strengths of the $\Delta D - s_R(t)$ and $\Delta D - t_{\text{burst}}$ correlations, respectively. We illustrate these “envelope” correlations in Fig. 14. We compute the “measured” $\text{EW}(\text{H}\alpha)$ and $(B-R)$, directly from the selected $(B-R)_0$, $s_R(t)$, and t_{burst} using the L99 models with either the steep or Salpeter IMF.

For several combinations of t_{max} , $s_{R,\text{max}}$, c_s and c_t , we repeat this procedure 1000 times and examine the average. We explore the ability of this procedure to reproduce values close to the averages, $\langle \text{EW}(\text{H}\alpha) \rangle$ and $\langle (B-R)_s \rangle$, of the data, corrected for extinction via the Calzetti, Kinney, & Storchi-Bergmann (1994) prescription (but not for nebular emission in this case); these averages are $\langle \text{EW}(\text{H}\alpha) \rangle = 61 \text{ \AA}$ and $\langle (B-R)_s \rangle = 0.71$, respectively. We also explore the relative strengths of the correlations we produced with this procedure using the Spearman rank probability as our measure of correlation. The correlation strengths for the data are somewhat ambiguous. Without reddening correction or correction for nebular line emission, the $\Delta D - \text{EW}(\text{H}\alpha)$ and $(B-R)_s$ correlations for these 72 galaxies have strengths of $P_{\text{SR}} = 0.0077$ and 0.033 , respectively. With the “Calzetti” correction, which introduces scatter through imprecision but also renders $(B-R)_s$ and $\text{EW}(\text{H}\alpha)$ more accurate, the strengths of the Spearman rank correlations diminish to $P_{\text{SR}} = 0.059$ and 0.165 , respectively. Because the appropriate values of P_{SR} are somewhat unclear, we require only that the average Spearman rank probabilities satisfy $0.006 \leq \langle P_{\text{SR}} \rangle \leq 0.06$ for the simulated $\Delta D - \text{EW}(\text{H}\alpha)$ distribution, that $0.02 \leq \langle P_{\text{SR}} \rangle \leq 0.2$ for the simulated $\Delta D - (B-R)_s$ distribution, and that the simulated $\Delta D - \text{EW}(\text{H}\alpha)$ relation is, on average, substantially more significant than the $\Delta D - (B-R)_s$ distribution averaged over the 1000 simulations.

Fig. 15a shows $\langle \text{EW}(\text{H}\alpha) \rangle$ and $\langle (B-R)_s \rangle$ resulting from the simulations that satisfy the requirements on $\langle P_{\text{SR}} \rangle$ for the $\Delta D - \text{EW}(\text{H}\alpha)$ and $\Delta D - (B-R)_s$ distributions. We test only values with $t_{\text{max}} \leq 900$ Myr. For all the tested Salpeter IMF bursts with the Peletier & Balcells (1996) distribution of $(B-R)_0$ colors, the simulations fail to match the observed $\langle \text{EW}(\text{H}\alpha) \rangle$ and $\langle (B-R)_s \rangle$. The most pressing problem is that the initial bulge colors are too red; the $\text{EW}(\text{H}\alpha)$ distribution requires weak Salpeter bursts for a match while the $(B-R)_s$ constraint requires strong bursts. The combination that comes closest to the measured range is that of strong ($s_{R,\text{max}} = 0.99$) but, on average, older bursts ($t_{\text{max}} = 900$ Myr). No simple adjustments to the input $\Delta D - \text{EW}(\text{H}\alpha)$ or $(B-R)_s$ correlations will suffice for $t_{\text{max}} \leq 900$ Myr. If the Peletier & Balcells (1996) colors indicate the appropriate distribution of $(B-R)_0$, the Salpeter bursts cannot reproduce the observations.

Salpeter-IMF bursts on a bluer $(B-R)_0$ distribution can meet with more success. We adopt the distribution of half-light colors from the Nearby Field Galaxy Survey of Jansen et al. (2000, NFGS), restricting to $M_B \leq -17$ (with magnitudes as published but adjusted for $H_0 = 70 \text{ km s}^{-1} \text{ Mpc}^{-1}$). Because colors are known to depend on M_B , we ensure that the color distribution drawn from the NFGS is appropriate for a sample with

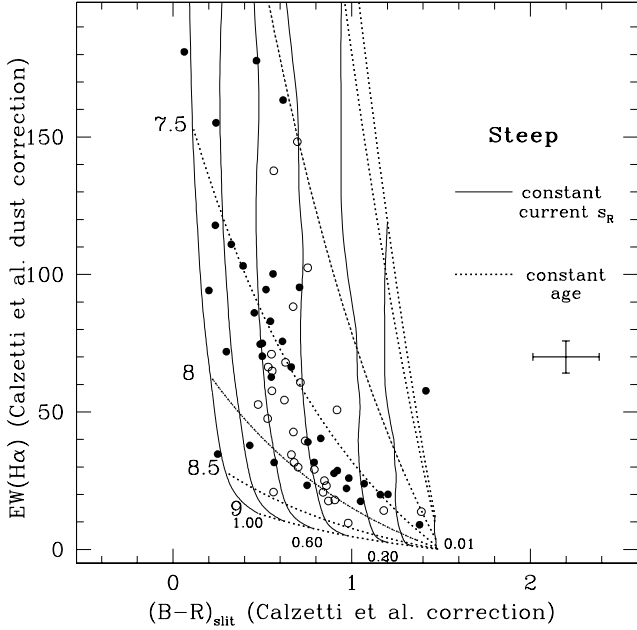


FIG. 13.— Similar to the panel in Fig. 11 with the “Calzetti” dust correction and the steep IMF. The points are segregated based on pair separation, ΔD ; filled circles are galaxies in pairs with $\Delta D < 20 h^{-1}$ kpc. Open circles have $\Delta D > 30 h^{-1}$ kpc. We omit the galaxies without measured Balmer decrements.

the M_B distribution of our pairs. To match the distributions, we draw M_B from the pair distribution; we then assign the galaxy a $(B-R)_0$ that equals the color of an NFGS galaxy selected randomly within the ± 10 galaxies closest in M_B . To take the most conservative approach, we correct the $(B-R)_0$ colors using Balmer decrements drawn from the pair sample, to match the $E(B-R)$ in the pair bursts. This approach is conservative as it is appropriate only if the reddening of the pre-interaction galaxies equals the reddening of the post-burst galaxies.

Fig. 15b shows the results from this algorithm. The Salpeter simulations with strong $s_{R,\max}$ and large t_{\max} reach the range of interest for some simulations with $t_{\max} = 700$ or 900 Myr and $s_{R,\max} = 0.8$. This maximum timescale is much larger than the expected dynamical timescales for ~ 50 kpc of separation on the sky. They may reflect some contamination in the $EW(H\alpha) > 15 \text{ \AA}$ pair population from galaxies with older bursts or no triggered bursts, but the Salpeter IMF also probably does not result in blue enough colors for the right range of $EW(H\alpha)$. We note that the prescription of correcting the $(B-R)_0$ colors based on the measured burst Balmer decrements in our pair sample is probably an overestimate of the reddening for the pre-existing stellar population. In addition, the NFGS does not explicitly eliminate galaxies in pairs and therefore already contains some triggered bursts. Finally, the $(B-R)_0$ color distribution we seek should include only the central few kpc of the galaxies, whereas the NFGS colors refer to the colors within the effective radius, frequently larger than the extraction area of our spectra; there is more blue disk contamination in the NFGS colors. Thus, only a conservatively blue $(B-R)_0$ color distribution reproduces the observations with the Salpeter IMFs, with what are probably unrealistically long timescales.

For the steep IMF, Fig. 15 shows that several combinations of parameters yield average $EW(H\alpha)$ and $(B-R)_s$ values in the appropriate range, for either $(B-R)_0$ distribution. The best-fitting

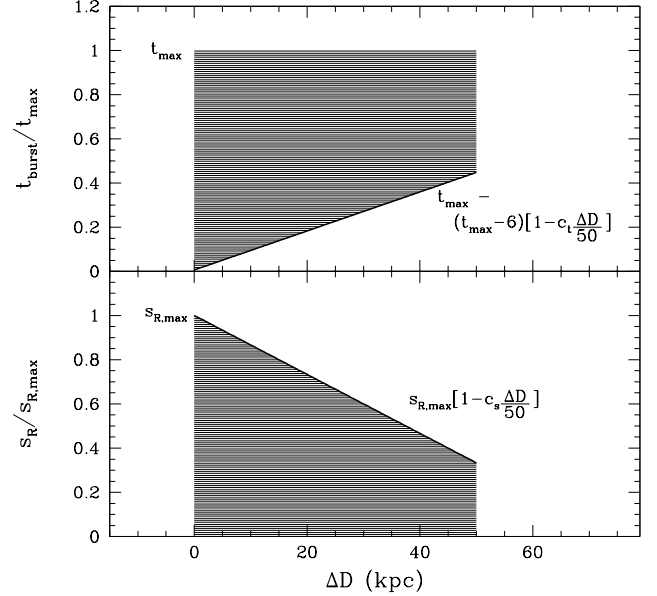


FIG. 14.— An illustration of the simulated “envelope” correlations we draw from to construct the 72-galaxy simulated data sets that we compare with the real data. For this figure, we use $c_t = 4/9$ and $c_s = 2/3$. The values we draw for the simulation are uniformly distributed in ΔD ; hence they are not drawn uniformly from the shaded region, but uniformly from the x-axis.

solutions we find all have $s_{\max} \geq 0.5$ and most have $s_{\max} \geq 0.8$. The solutions work well for a range of c_s and c_t values; all require relatively strong $\Delta D - s_R(t)$ correlations, with $c_s > 0.33$. However, the resulting timescales, with $t_{\max} = 50 - 100$ Myr, are unrealistically short. We therefore speculate that an IMF steeper than Salpeter, but shallower than the “steep” IMF we employ here, would probably provide the best match to the data with the most realistic timescales and assumptions.

With the Peletier & Balcells (1996) bulge colors for the $(B-R)_0$ distribution, the best-fitting solutions all have $\Delta D - (B-R)_s$ and $\Delta D - EW(H\alpha)$ correlations (with $c_s \geq 1/3$ and $c_t \geq 1/3$ for the solutions shown). However, for the bluer NFGS $(B-R)_0$ colors, 1 of the 13 indicated “steep IMF” solutions that fall within the indicated region has $c_t = 0$. Thus, a $\Delta D - t_{\text{burst}}$ correlation is not strictly required to reproduce the data.

The Monte Carlo simulation is not a rigorous attempt to reproduce the data but a simple exploration of the different combinations of continuous bursts of star formation which can result in the appropriate $\Delta D - EW(H\alpha) - (B-R)_s$ distribution. We conclude that the result depends on the appropriate distribution of $(B-R)_0$ for the particular sample. If the Peletier & Balcells (1996) bulge colors are appropriate, the models require a high-mass IMF that is substantially steeper than Salpeter to explain the observed colors, equivalent widths, and $\Delta D - EW(H\alpha)$ correlation using simple star formation histories. Adopting much bluer progenitor colors does allow the Salpeter-IMF bursts to fit our model, but the required colors may be too blue to be realistic. Our data indicate a burst IMF steeper than Salpeter, but probably not as steep as $\alpha = -3.3$.

Regardless of IMF, the models explain the observed $\Delta D - EW(H\alpha)$ correlation only if there is a strong correlation between pair separation on the sky and the fraction of R -band flux in the spectroscopic aperture that originates from the new burst

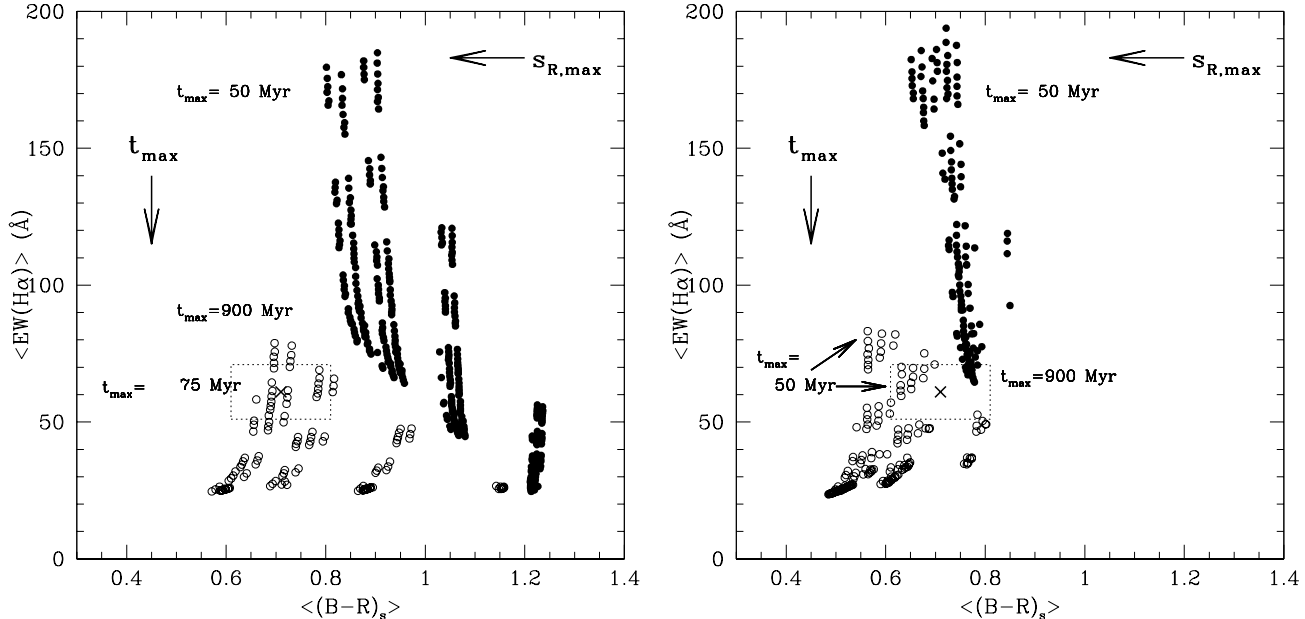


FIG. 15.— Monte Carlo results using the $(B-R)_0$ distribution of Peletier & Balcells (1996) (*left*), and from the NFGS $(B-R)_0$ distribution prescription (*right*) for which we draw $(B-R)_0$ colors based on M_B (see text). Solid points are Salpeter models; open circles show results using the steep IMF. The box indicates the region surrounding the sample average measurements (x), $\langle \text{EW}(\text{H}\alpha) \rangle = 61 \text{ \AA} (\pm 10 \text{ \AA})$ and $\langle (B-R)_s \rangle = 0.71 (\pm 0.1)$, both corrected for reddening via the “Calzetti” reddening prescription. The points show Monte Carlo results for $s_{R,\text{max}} = 0.2, 0.5, 0.8,$ and 0.99 (*generally left to right*), and $t_{\text{max}} = 50, 100, 200, 300, 500, 700,$ and 900 Myr (*generally top to bottom*), omitting combinations that result in very small $\langle \text{EW}(\text{H}\alpha) \rangle$. We add $t_{\text{max}} = 75$ Myr for the Peletier & Balcells (1996) colors and steep IMF, to illustrate that the results coincide directly with the data. Considering values of c_s and c_t from 0 to 1 (in increments of $1/9$), we show only results that satisfy the Spearman rank correlation properties described in the text.

(i.e., a strong $\Delta D - s_R(t)$ correlation). Most, but not all, of the working models also require a strong $\Delta D - t_{\text{burst}}$ correlation. The models which do not require the $\Delta D - t_{\text{burst}}$ correlation represent a departure from the models of BGK, which explain the $\Delta D - \text{EW}(\text{H}\alpha)$ correlation with a $\Delta D - t_{\text{burst}}$ correlation only. However, as we note, a substantial $\Delta D - t_{\text{burst}}$ relationship is still consistent with the data (and predicted by most of the models we explore). If the correlation still plays some role, then the interpretation of BGK still holds qualitatively, but with somewhat shorter timescales than BGK discuss (e.g., by factors of 1.5–3). We require additional data (e.g., near-infrared) to verify the relative roles of the $\Delta D - t_{\text{burst}}$ and $\Delta D - s_R(t)$ correlations.

5. CONDITIONS THAT AFFECT THE STRENGTHS AND AGES OF THE BURSTS

Although we lack direct constraints on $(B-R)_0$ we briefly investigate the relationships between third parameters and star formation more rigorously by inverting $\text{EW}(\text{H}\alpha)_{\text{meas}}(t)$ and $(B-R)_s$ to measure the burst age, t_{burst} , and strength, $s_R(t)$. Several observational problems complicate this process. First, not every galaxy in the $(B-R)_s/\text{EW}(\text{H}\alpha)_{\text{meas}}(t)$ plane has a valid solution for every model. We omit galaxies with ages $> 10^9$ years. For the two galaxies with nominal $s_R(t) > 1$ we define $s_R(t) = 0.999$ and estimate t_{burst} by increasing the measured color until a valid solution exists; this procedure corresponds to moving the points to the right on Fig. 11, into the edge of the region of valid solutions. Second, uncertainties in $(B-R)_0$ plague this analysis; we focus primarily on models with constant $(B-R)_0$ and models with a linear dependence of $(B-R)_0$ on the log of the rotation speed of the galaxy. The final observational problem results from incompleteness in the sample of galaxies with mea-

sured Balmer decrements (hence accurate corrected colors and equivalent widths); this sub-sample becomes incomplete for $\text{EW}(\text{H}\alpha)_{\text{meas}}(t) \lesssim 20 \text{ \AA}$ (see Fig. 6). As a result of this incompleteness, the data are not sampled uniformly in t_{burst} or $s_R(t)$. We explore possible correlations between third parameters and t_{burst} and/or $s_R(t)$ after truncating the sample in accordance with this approximate incompleteness limit. There are many acceptable combinations of cutoff $s_R(t)$ and t_{burst} that result in different sub-sample sizes. We explore two sub-samples: (1) $s_R(t) > 0.3$, $t_{\text{burst}} < 10^8$ years, and (2) $s_R(t) > 0.4$, $t_{\text{burst}} < 10^{8.2}$ years. Table 5 lists the number of galaxies with valid solutions in the subsets we consider, including the full sample, the full sample restricted to galaxies with measured Balmer decrements, and these complete sub-samples. The table notes additional prescriptions for $(B-R)_0$ that we describe in Sec. 5.2, and indicates the number of galaxies that have measured velocity widths, $V_{2.2}^c$.

5.1. $s_R(t)$, t_{burst} , and the Orbit Parameters

Fig. 16 shows the burst strength and age solutions assuming a constant $(B-R)_0 = 1.5$. We show all the galaxies with valid solutions with the steep IMF and the “Calzetti” reddening correction. We plot burst $s_R(t)$ and age, t_{burst} , as functions of ΔD and ΔV . The filled circles are the galaxies with measured Balmer decrements within the complete sub-sample restricted to galaxies with $s_R(t) > 0.4$ and $t_{\text{burst}} < 10^{8.2}$ years. The open circles indicate galaxies with solutions outside of the complete range and/or galaxies with no measured Balmer decrement. The typical formal error in $s_R(t)$ is ~ 0.2 for $0.2 \lesssim s_R(t) \lesssim 0.6$ and is somewhat larger for other strengths. Errors in burst age are correlated with the burst strengths of the galaxies. For most galaxies, errors are $\sim 0.2 - 0.3$ dex; however, for galaxies with $s_R(t) \lesssim 0.2$ the age errors can span several dex (see Fig. 11).

TABLE 4
NUMBER OF GALAXIES WITH VALID MODEL SOLUTIONS FOR SUBSETS OF THE DATA

Prescriptions		Number with Valid Solutions			
$(B-R)_0$	Reddening	Full Sample	With	Complete ^a	Complete ^a
			Measured $H\alpha/H\beta$	($t_{\text{burst}} < 10^{8.2}$ yr) ($s_R(t) > 0.4$)	($t_{\text{burst}} < 10^8$ yr) ($s_R(t) > 0.3$)
$(B-R)_0 = 1.5$	“Calzetti”	131	77	43	51
$(B-R)_0 = 1.5+$	“Calzetti”	68	35	12	16
$1.5[\log V_{2.2}^c - 2.5]^b$					
$(B-R)_0 = 1.5+$	“Calzetti”	74	39	15	20
$0.75[\log V_{2.2}^c - 2.5]^b$					
$(B-R)_0 = 1.5$	none	114	75	17	28
$(B-R)_0 = 1.5+$	none	57	31	1	5
$1.5[\log V_{2.2}^c - 2.5]^b$					
$(B-R)_0 = 1.5+$	none	62	37	3	8
$0.75[\log V_{2.2}^c - 2.5]^b$					
Prescriptions		Number with Valid Solutions and Measured $V_{2.2}^c$			
$(B-R)_0 = 1.5$	“Calzetti”	72	39	17	21
$(B-R)_0 = 1.5$	none	61	38	6	11

^aSubsample in a “complete” region of $t_{\text{burst}} - s_R(t)$ space that includes only galaxies with measured Balmer decrements.

^bAll galaxies in these categories have a measured $V_{2.2}^c$.

The only visually evident correlation among the 43 solid points in Fig. 16 (complete sample) is the absence of very strong bursts with large separations. However, Spearman rank tests confirm both a tendency for galaxies with smaller separations to have younger burst ages ($P_{SR} = 0.030$) and for galaxies with smaller separations to have stronger bursts ($P_{SR} = 0.033$). The other parameter combinations show no correlations, with $P_{SR} = 0.17$ and 0.76 for the $t - \Delta V$, and $s_R(t) - \Delta V$ plots, respectively. If we instead adopt $t_{\text{burst}} = 10^8$ years and $s_R(t) = 0.3$ as our completeness limits, the significance of the $\Delta D - t_{\text{burst}}$ correlation increases to $P_{SR} = 0.0019$; the significance of the $\Delta D - s_R(t)$ correlation also increases slightly, to $P_{SR} = 0.012$. With the inclusion of the galaxies that lack measured Balmer decrements or that fall in the incomplete parts of the sample (open circles), a significant correlations persists between ΔD and $s_R(t)$ ($P_{SR} = 0.038$) while the significance of the $\Delta D - t_{\text{burst}}$ dependence drops to $P_{SR} = 0.12$.

5.2. $(B-R)_0$, $s_R(t)$, t_{burst} , and the Intrinsic Properties of the Progenitor Galaxies

Sec. 4 examines general trends in the star formation timescales and orbital parameters of galaxies in pairs. Uncertainties in the properties of the progenitor galaxies, in the IMF of the triggered bursts, and in the reddening corrections complicate the interpretation of these apparent trends. Even if a theoretically tight relationship exists between the triggered star formation properties and the positions of the galaxies in their orbits, we still expect variations in the progenitor galaxies (mass, orbit, environment, star formation history, IMF). These variations add to scatter introduced by interlopers ($\sim 10\%$; see BGK), by galaxies that have not had a close pass yet, and by the accessibility of only two components of the true spatial ΔD and one of the true ΔV .

One powerful tool for sorting out the causes of the large

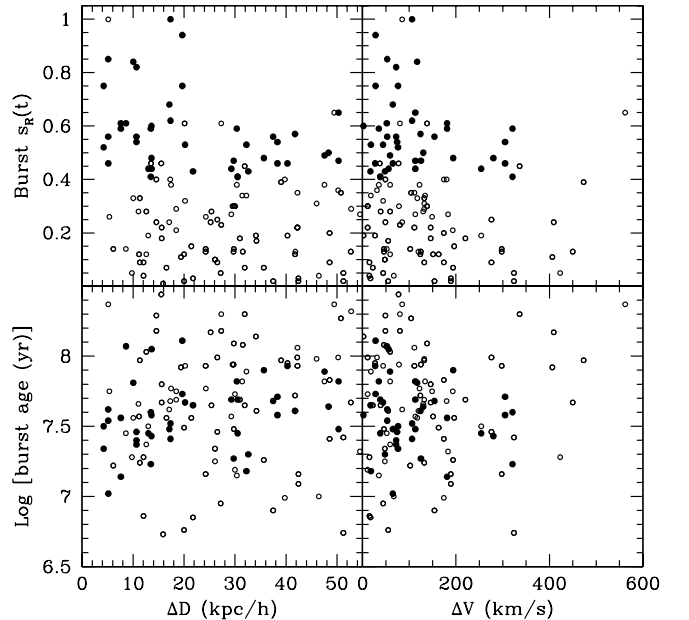


FIG. 16.— Burst parameters ($s_R(t)$, and age, t , assuming $(B-R)_0 = 1.5$) vs. pair orbit parameters, ΔD and ΔV , for the galaxies with valid solutions only. Solid points represent the 43 galaxies in the complete sub-sample (excluding one point with $\Delta D = 76 \text{ h}^{-1} \text{ kpc}$ from the left panels); they have measured Balmer decrements with burst ages $t < 10^{8.2}$ years and strengths $s_R(t) > 0.4$. We plot the points without measured Balmer decrements and/or without valid solutions within the complete region as open circles. Within the complete sub-sample, there is a tendency for galaxies with smaller values of ΔD to have younger burst ages ($P_{SR} = 0.030$) and stronger bursts ($P_{SR} = 0.033$).

scatter we find in Sec. 5.1 is the search for dependence of the amount and kind of interaction-triggered star formation on third

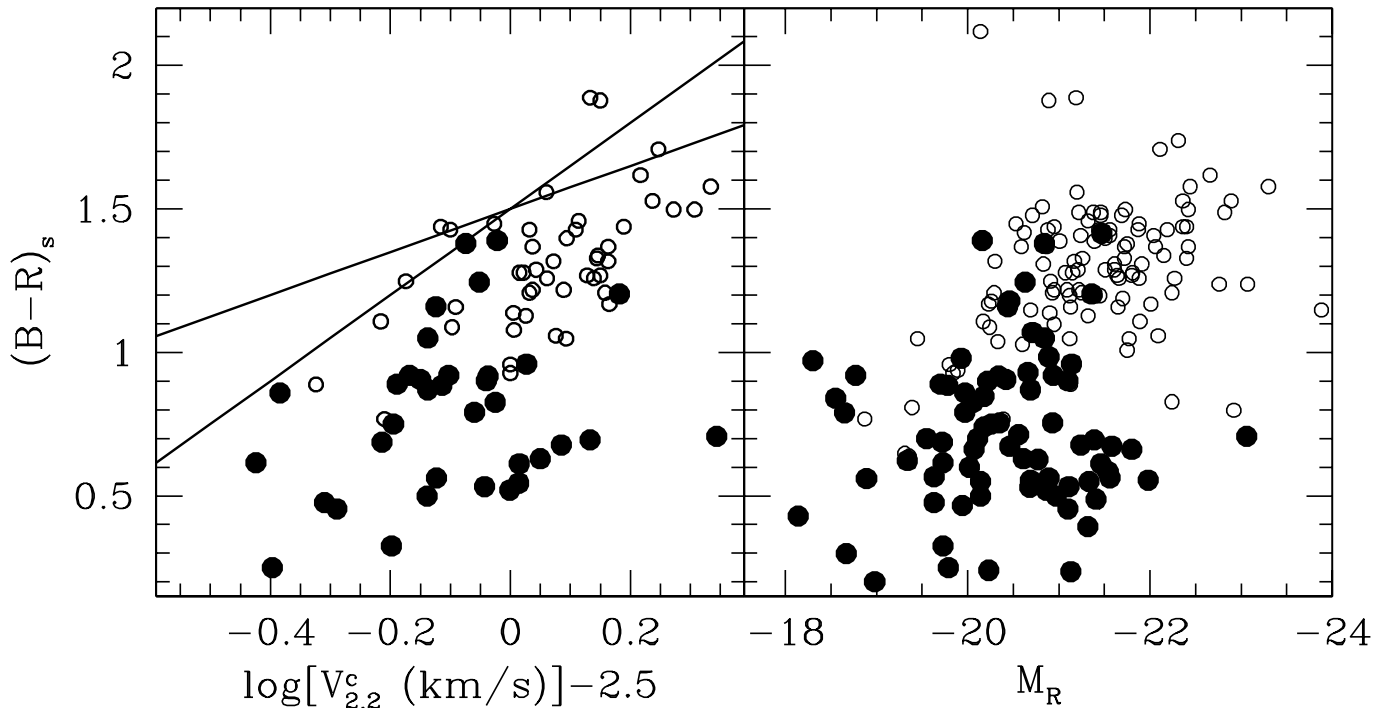


FIG. 17. — $(B-R)_s$ corrected for reddening and nebular lines (*left*) as a function of rotation curve velocity width and (*right*) R-band total magnitude for all galaxies in the SP sample. We segregate galaxies into groups with measured (solid points) or unmeasured (open points) Balmer decrements. The solid lines indicate the two prescriptions we adopt for $(B-R)_0$ as a function of $V_{2,2}^c$.

parameters (e.g., Tissera et al. 2002). In this section, we explore the possible dependence of $(B-R)_0$ on intrinsic luminosity and rotation speed, and the relationships between burst parameters and the velocity widths of the galaxies.

Galaxy colors depend strongly on luminosity, as exhibited by the different Tully-Fisher slopes observed for different band-passes (see e.g., Tully, Mould, & Aaronson 1982; Tully & Pierce 2000; Bell & de Jong 2001). However, estimates in the literature vary widely and depend on the particular velocity width measure. Tully & Pierce (2000) find a difference of only ~ 0.3 magnitudes per dex; Bell & de Jong (2001) quote differences from 0.67 to 1.05 magnitudes per dex, depending on the reddening prescription. We concern ourselves only with the colors measured in the central (spectroscopic) apertures of the target galaxies. Thus, the extensive Tully-Fisher studies in the literature are of limited use. We rely on empirical estimates of the probable range of variations in color with rotation speed. Fig. 17 shows $(B-R)_s$, corrected for reddening with the “Calzetti” prescription, as a function of velocity width, for galaxies with well-measured rotation curves, and as a function of M_R for all the SP galaxies. [See Barton et al. (2001) for the definition of the velocity width, which we measure from the major axis rotation curves.] The figure clearly shows the dependence of color on luminosity or rotation speed; the probable dependence of $(B-R)_0$ on luminosity and rotation speed follows.

To test the effects of allowing $(B-R)_0$ to vary with velocity width, we adopt the $(B-R)_0$ relations drawn in Fig. 17a. The lines correspond to $(B-R)_0 = 1.5 + 1.5 [\log V_{2,2}^c - 2.5]$ and $(B-R)_0 = 1.5 + 0.75 [\log V_{2,2}^c - 2.5]$. Using these prescriptions, we find that almost all of the correlations in Sec. 5.1 have been

reduced in significance. The reduced sample size (from 43–51 to 12–20 galaxies; see Table 5) probably contributes to this reduction in significance. We note that a $\Delta D - t_{\text{burst}}$ correlation persists, with $P_{\text{SR}} = 0.034$, if we assume $(B-R)_0 = 1.5 + 0.75 [\log V_{2,2}^c - 2.5]$ and only accept solutions with $t_{\text{burst}} < 10^8$ years and $s_R(t) > 0.3$. For the “complete” subsample with the same limits but with $(B-R)_0 = 1.5 + 1.5 [\log V_{2,2}^c - 2.5]$, the correlation disappears, with $P_{\text{SR}} = 0.17$. For the other “complete” subsample, these correlations also disappear, with $P_{\text{SR}} = 0.18$ and 0.33 for the two $(B-R)_0$ prescriptions. Curiously, we also note marginal correlations between ΔV and $s_R(t)$ for various restricted sub-samples.

The metallicities, emission line equivalent widths, and dust content of galaxies all depend on mass and/or luminosity (e.g., Tully, Mould, & Aaronson 1982; Skillman, Kennicutt, & Hodge 1989; Heckman et al. 1998; Carter et al. 2001; Jansen, Franx, & Fabricant 2001). The required reddening correction thus depends on luminosity and rotation speed (e.g., Wang & Heckman 1996; Tully et al. 1998; Sullivan et al. 2001; Hopkins et al. 2001). Fig. 18 illustrates this very significant dependence in the SP sample. The true fractional strengths of bursts of star formation in these galaxies may also depend on mass. Some trends with mass or luminosity appear to extend to the triggered star formation; in the BGK pair sample, the galaxies with the largest measured values of $\text{EW}(\text{H}\alpha)$ are the lower-mass, lower-luminosity galaxies. Barton et al. (2001) find a shallow slope of the Tully-Fisher relation for these pairs.

Here, we test for the dependence of the strengths and ages of triggered bursts of star formation on the masses (rotation speeds) and luminosities of the progenitor galaxies. Timescales for tidally-triggered star formation are much shorter than a

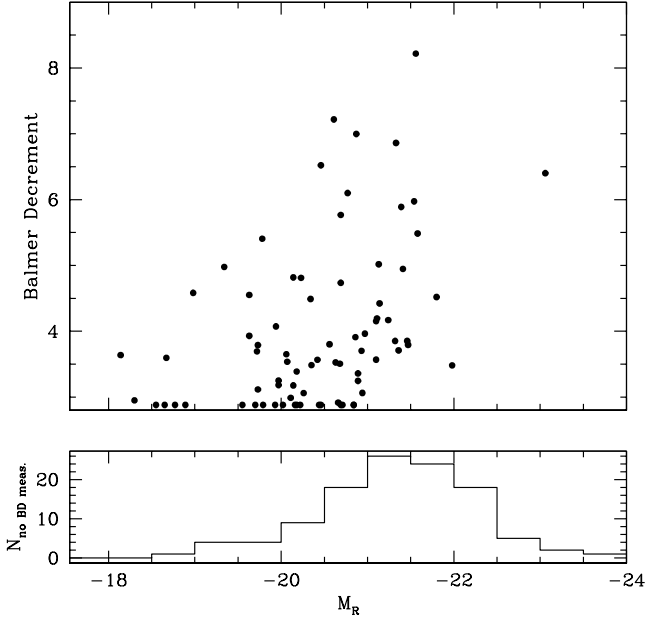


FIG. 18.— Balmer decrement as a function of R-band luminosity for (top) the 78 galaxies with measured Balmer decrements. The data show a tendency for more luminous galaxies to harbor more dust ($P_{\text{SR}} = 7.1 \times 10^{-5}$). The histogram shows the 112 galaxies with $H\beta$ emission too weak to measure the Balmer decrement. These galaxies tend to be luminous. The histogram in Fig. 6 shows their $\text{EW}(H\alpha)$ distribution.

Hubble time. Thus, even if the frequency of interaction depends on mass, a large enough, unbiased set of galaxies in pairs should show no dependence of burst age on stable (non-transient) properties like progenitor mass. The Spearman rank test indicates, as expected, no dependence of burst age on rotation speed within the 17-galaxy complete sub-sample (see Table 5) when we assume a fixed $(B-R)_0 = 1.5$ (although a correlation does exist between galaxy R-band absolute magnitude, M_R , and t_{burst} , with $P_{\text{SR}} = 0.011$ or 0.031 , depending on the complete sub-sample). We introduce very strong false correlations when we include galaxies in the incomplete region of $t_{\text{burst}} - s_{\text{R}}(t)$ space or galaxies without measured Balmer decrements; with the “Calzetti” extinction correction the significance is $P_{\text{SR}} = 0.0014$. The complete sample with no dust corrections is too small to test for a significant correlation. The correlation including all the points in the no-dust-correction scenario is very strong ($P_{\text{SR}} = 3.1 \times 10^{-6}$). Thus we conclude that restriction of the sample to the complete sub-sample and the correction for dust are very important for eliminating artificial systematic trends (see Fig. 18). Our prescription for changing $(B-R)_0$ as a function of $V_{2,2}^c$ also eliminates most of the artificial dependence of burst age on rotation velocity.

Although correlations between galaxy mass and burst age are almost certainly unphysical, a correlation between mass and burst strength could be real. The low-mass galaxies clearly tend to have bluer colors and higher $\text{EW}(H\alpha)$ values than the higher-mass galaxies. We investigate the solutions in detail, solving directly for the burst strengths and ages. We find some statistical evidence that the suggested correlation between rotation velocity and burst strength exists. Assuming a constant $(B-R)_0 = 1.5$, significant correlations exist both within the restricted, robust, complete sub-sample and for all of the data (including the galaxies with no measured Balmer decre-

ment). With a “Calzetti” dust correction the Spearman rank probability is $P_{\text{SR}} = 0.035$ for the complete sample (restricted to $t_{\text{burst}} < 10^{8.2}$ years, $s_{\text{R}}(t) < 0.4$; 17 galaxies), although it is only $P_{\text{SR}} = 0.086$ for the other complete sub-sample. The complete no-dust-correction sample is too small to test for a significant correlation. However, including all the galaxies with valid solutions, measured $V_{2,2}^c$, and no dust correction, the Spearman rank probability is $P_{\text{SR}} = 4.0 \times 10^{-11}$. Because these are the prescriptions for which the unphysical burst age-luminosity and burst age-rotation speed correlations are strong, however, systematic problems introduced by incompleteness and the lack of knowledge of the true $(B-R)_0$ almost certainly affect interpretation of the results.

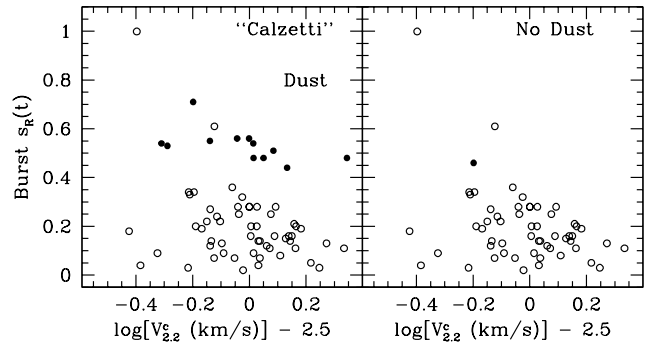


FIG. 19.— Current burst strength for $(B-R)_0 = 1.5 + 1.5 \times [\log V_{2,2}^c - 2.5]$ as a function of rotation speed with (left) a “Calzetti” dust correction and (right) no dust correction. The small number of filled circles have measured Balmer decrements and valid age and strength solutions within a “complete region” ($t < 10^{8.2}$ years, $s_{\text{R}}(t) > 0.4$); open circles have no measured Balmer decrement and/or solutions outside the complete region.

We test the robustness of the apparent burst strength-rotation speed correlation by assuming the prescriptions for $(B-R)_0$ with $V_{2,2}^c$ that we describe above. If we assume $(B-R)_0 = 1.5 + 0.75[\log V_{2,2}^c - 2.5]$ and “Calzetti” reddening, the complete sub-sample with $t_{\text{burst}} < 10^{8.2}$ years and $s_{\text{R}}(t) < 0.4$ yields a significant $V_{2,2}^c - s_{\text{R}}(t)$ correlation ($P_{\text{SR}} = 0.0023$). Restriction to the other sub-sample yields no correlation, however. For $(B-R)_0 = 1.5 + 1.5[\log V_{2,2}^c - 2.5]$ (see Fig. 19), the $V_{2,2}^c - s_{\text{R}}(t)$ correlation remains significant for “Calzetti” dust ($P_{\text{SR}} = 0.011$); again, we observe no correlations within the second complete sub-sample. Inclusion of the points outside the complete sub-sample yields $P_{\text{SR}} = 0.49$ (35 galaxies) and including the additional points without measured Balmer decrements yields $P_{\text{SR}} = 0.10$ (for 68 galaxies). The correlation among all galaxies in Fig. 19b is significant, with $P_{\text{SR}} = 3.2 \times 10^{-4}$. We note that of all the combinations we consider in which $(B-R)_0$ depends on $V_{2,2}^c$, artificial $V_{2,2}^c - t_{\text{burst}}$ correlations are only found using the $(B-R)_0$ relation with a slope of 0.75 with no dust corrections.

The relationship between $V_{2,2}^c$ and the true masses of galaxies is not straightforward, especially for interacting galaxies with centrally-concentrated star formation. Barton et al. (2001) find several examples of galaxies with truncated rotation curves that have anomalously small velocity widths. When analyzed from the perspective of another measure of intrinsic galaxy mass, M_R , the data do not present a particularly consistent picture. For example, with a constant $(B-R)_0 = 1.5$, we find no significant burst strength-luminosity correlations in the complete subsets of the data. When we restrict again to galaxies with measured

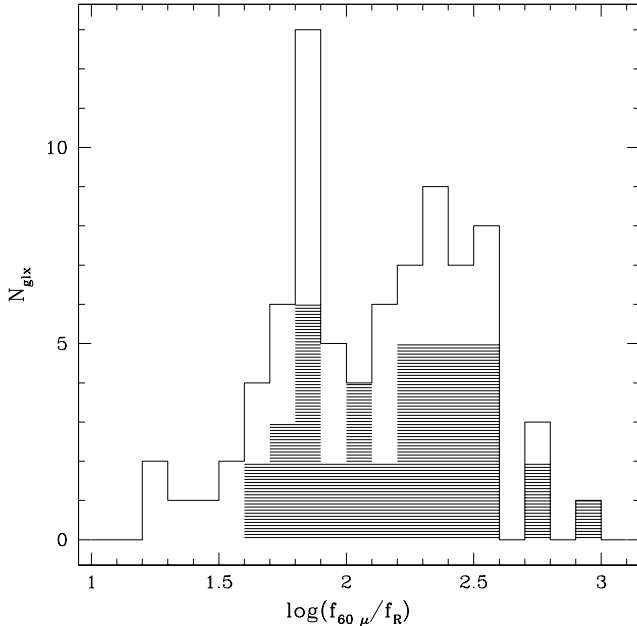


FIG. 20.— For the IRAS psc catalog detections, we plot a histogram of the log of the ratio of the total IRAS $60\ \mu\text{m}$ flux within $3'$ of the galaxy to the R -band luminosity. We note that in some cases the IRAS flux includes flux from both galaxies. The shaded histogram includes only the galaxies with measured Balmer decrements (42 galaxies); the main histogram includes all galaxies with IRAS detections (120 galaxies). A K-S test indicates only marginally significant differences, at best, in the distributions, with $P_{\text{KS}} = 0.12$.

$V_{2.2}^c$ and assume either of the relations between $(B-R)_0$ and $V_{2.2}^c$ we find a significant $s_{\text{R}}(t) - M_{\text{R}}$ correlation for one of the complete sub-sample with $t_{\text{burst}} < 10^{8.2}$ and $s_{\text{R}}(t) > 0.4$. In addition, we note that there are unphysical $M_{\text{R}} - t_{\text{burst}}$ correlations, even among the complete sub-samples. We do note a strong tendency for galaxies with lower metallicities to have stronger bursts. Although we use solar metallicity for all of the bursts described here, our tests reveal that the use of lower metallicity models for the low metallicity galaxies and higher metallicity models for the higher metallicity galaxies would only enhance this correlation, as the better-suited models result in stronger bursts at low metallicity and weaker bursts at high metallicity. We plan to explore these relationships in more detail in the future.

Our analysis, though far from conclusive, suggests that more luminous galaxies may experience weaker fractional bursts of star formation. However, as Heckman et al. (1998) point out and as Fig. 18 shows, more massive galaxies are more dust-rich. Strong dust-enshrouded bursts may hide among the luminous galaxies for which we are unable to measure a Balmer decrement. Hence the apparent conclusion (here and elsewhere) that less massive galaxies have higher luminosity-weighted star formation rates may be an artifact of inadequate correction for extinction.

The IRAS point source catalog provides a method of searching for strong starbursts embedded in the luminous galaxies. Because the IRAS beam is large, we sum all flux within $3'$ of the optical galaxy, including the flux for both galaxies in many close pairs. Thus, these ratios are actually upper limits. Fig. 20 shows the distribution of the IRAS $60\ \mu\text{m}$ -flux-to- R -band luminosity ratios for the IRAS-detected sample with measured Balmer decrements (37/78 detected; shaded histogram) and the

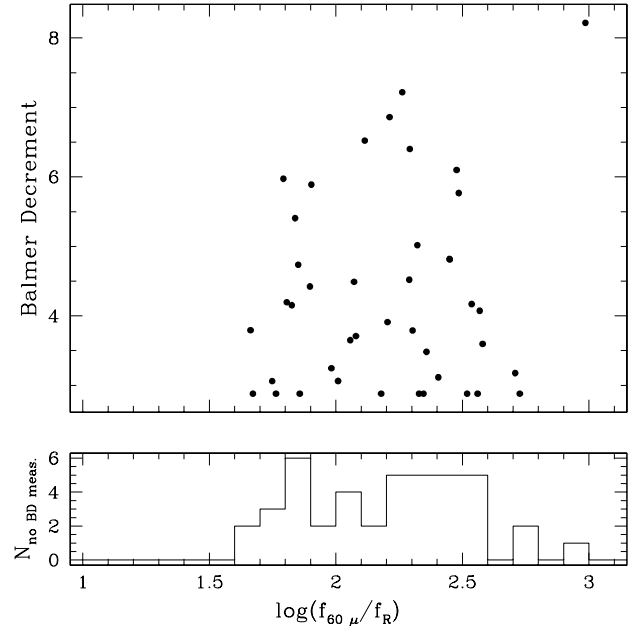


FIG. 21.— The relationship between Balmer decrement and the $60\ \mu\text{m}$ -to- R -band flux for IRAS-detected galaxies in pairs (see Fig. 20.) The bottom histogram is the distribution of flux ratios for galaxies without measured Balmer decrements.

sample as a whole (79/190 detected; open histogram). The distributions are at best marginally different, with $P_{\text{KS}} = 0.12$. We find no evidence for extreme hidden starbursts among the galaxies with small $\text{EW}(\text{H}\alpha)$ (hence without measured Balmer decrements).

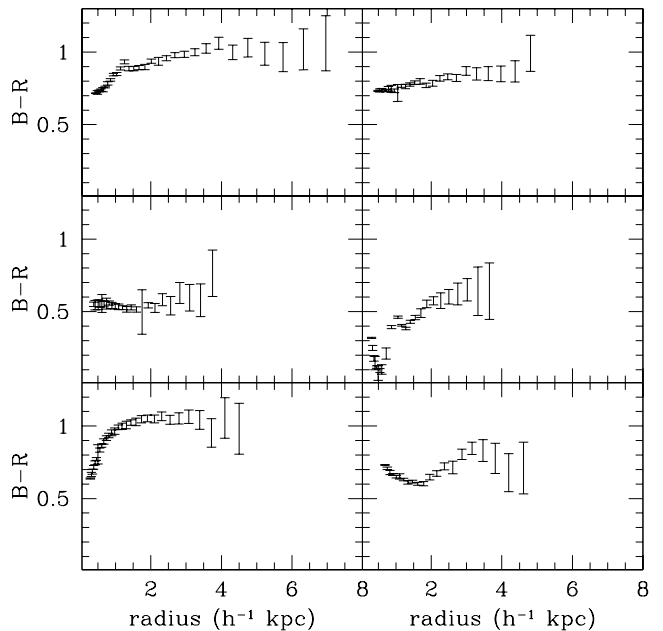


FIG. 22.— Color profiles of the 6 galaxies with $s_{\text{R}}(t) > 0.8$ (assuming $(B-R)_0 = 1.5$, the steep IMF, and the “Calzetti” reddening prescription). These galaxies and many others with strong central star formation show blue dips in or near their centers; few of the galaxies are accompanied by tidal tails, although some companions have tails. Fig. 23 identifies the galaxies and shows B -band images.

We use Fig. 21 to estimate the possible effects of hidden bursts of star formation on the sample of galaxies without measured Balmer decrements. Based on the rest of the sample, their Balmer decrements are probably in the range of 2.88 – 8, appropriate for the far-IR range in our sample. Thus, the “Calzetti” corrections to the $B-R$ color and $EW(H\alpha)$ may be as large as ~ 0.83 magnitudes and a factor of 2.5, respectively, for the galaxies with the greatest amounts of dust. Although they cannot affect the correlations among the galaxies in the sample with measured Balmer decrements, more accurate dust corrections could move the open points in Fig. 19 to much greater strengths, reducing the significance of the observed $V_{2,2}^c - s_R(t)$ correlation. Thus, although the IRAS data argue against extremely strong hidden starbursts, they do not rule out subtle systematic dependences between galaxy luminosity and dust content that could give rise to a false correlation between burst strength and galaxy mass.

In summary, we find some evidence that triggered star formation may be (fractionally) stronger in lower-mass galaxies. This result, if confirmed, would provide one possible mechanism for the stronger star formation that is typically observed in lower-mass galaxies. However, we find much less evidence for this trend when we replace $V_{2,2}^c$ with M_R as a measure of the intrinsic mass of a galaxy. In addition, known systematic trends in the dust content and the stellar populations as a function of rotation speed or luminosity of the progenitor galaxies may be affecting our results. More accurate measures of the dust corrections and pre-existing stellar population colors are required to explore these issues further.

6. THE GALAXIES WITH STRONG CENTRAL STAR FORMATION

As one product of the analyses we implement in this paper, we use the $(B-R)_s/EW(H\alpha)_{\text{meas}}(t)$ plane to identify populations of galaxies with particularly strong bursts or in particular stages of interaction. Fig. 22 shows the $B-R$ color profiles of galaxies with convincing evidence for strong tidally-triggered bursts. These six galaxies have $s_R(t) > 0.8$ using the steep IMF and the “Calzetti” dust correction. We show images of the galaxies in Fig. 23.

The profiles show blue dips in or near the centers; these dips are frequent in our sample. By-eye estimates indicate that 22/185 (12%) of the luminous ($M_B \leq -17$) non-AGN galaxies have blue central dips in the SP sample. In contrast, the NFGS contains only 8/147 (5%) of luminous galaxies with blue central dips. Because pairs were not explicitly excluded by the NFGS, some of the dips in the NFGS sample may also result from interactions.

The SPH simulations of Mihos & Hernquist (1996) predict gas infall and centrally-concentrated star formation for bulgeless galaxies in the early stages of interactions (see the discussion in BGK). This centrally concentrated star formation has implications for the overall structural parameters of the galaxies, especially at higher redshifts where low-surface-brightness features are difficult to detect. Barton et al. (2001) and Barton & van Zee (2001) study the *transient* effects of central star formation on emission-line velocity widths and half light radii. They find a small number of outliers to the Tully-Fisher relation in the BGK sample with very narrow linewidths for their luminosities. Follow-up HI observations with the VLA reveal that the radio linewidths of these galaxies are much broader; the narrow optical line widths result from poor sampling of only the

central parts of the rotation curves. Barton & van Zee (2001) demonstrate that centrally concentrated star formation also artificially reduces the half-light radii of galaxies. Thus measures of linewidths and radii may lead to underestimates of the intrinsic masses and sizes of star-forming objects.

Although they exhibit triggered star formation and unusual, lumpy morphologies, the target galaxies in Fig. 23 have no long tidal tails. At best, 2/6 have very stubby possible tails. Numerical simulations demonstrate that tidal tails are transient and occur only in prograde interactions (Toomre & Toomre 1972). Thus, studies that identify interactions on the basis of the presence or absence of tidal tails are incomplete.

Our analyses also provide a method of identifying galaxies that have already undergone a close pass and are slowing down for a second pass or merger. We select galaxies that have been experiencing a long-lived but ongoing burst of star formation and are near apogalacticon by choosing galaxies with blue colors [here, $(B-R)_s^c < 0.75$], moderate $EW(H\alpha)$ [$20 \text{ \AA} < EW(H\alpha) < 40 \text{ \AA}$] indicative of a substantial build-up of R-band continuum, and small velocity separations ($\Delta V < 150 \text{ km s}^{-1}$). The morphologies of the chosen pairs suggest that this method is nearly 100% successful at identifying galaxies that have already experienced a close pass. We show B -band images of the pairs in Fig. 24; one of the galaxies overlaps with the strong-burst sample of Fig. 23. Of the 7 galaxies we select with these criteria, which are members of 7 different pairs, each pair shows one or more relatively unambiguous indication of a previous close pass (e.g., lumpy, unusual morphology or a tidal tail either in the blue galaxy itself or in the neighbor). A large sample of galaxy pairs near apogalacticon chosen in this manner would provide kinematic constraints on the dark matter content of galaxies (e.g., Charlton & Salpeter 1991).

7. CONCLUSION

We combine B and R photometry with longslit and central spectroscopy to explore the strengths and ages of tidally-triggered bursts of star formation in galaxies in pairs. We construct a two-population description of the pre-existing and triggered stellar populations near the centers of the galaxies. Our primary conclusions are:

1. The most realistic starburst models that describe the data statistically include continuous star formation, a steep (or truncated Salpeter) IMF, and the reddening correction of Calzetti, Kinney, & Storchi-Bergmann (1994). Consistency with the Salpeter IMF requires a very blue distribution of progenitor-galaxy colors.
2. In our picture, the models require strong triggered bursts in some of the pair galaxies; these bursts constitute $\gtrsim 50\%$ of the central R-band light. This star formation leads to a high incidence of galaxies with blue centers; tidal tails do not always accompany these central bursts of star formation.
3. Our results suggest that the strengths, and most likely the ages, of triggered bursts of star formation depend on the galaxy separation on the sky. Thus, although they do not conclusively verify the model, our data are consistent with the picture of a burst of star formation triggered by a close galaxy-galaxy pass that continues and ages as the galaxies move apart. In this picture, the strongest bursts of star

formation occur only in the tightest orbits, giving rise to the strength-separation correlations. The data also suggest a possible correlation between the strength of a triggered burst and the rotation speed (mass) of the progenitor galaxy, in the sense that low-mass galaxies experience stronger bursts of triggered star formation. This result supports the hypothesis that the evolution of galaxies is mass-dependent. Verifying these conclusions requires additional constraints on the colors and dust content of the pre-existing stellar populations.

The colors of the pre-existing stellar populations and the reddening corrections are the dominant uncertainties affecting conclusion (3). More accurate characterization of the correlations between orbit parameters and star formation properties in tidally interacting galaxies requires independent constraints on the colors of the old stellar populations. Near-IR observations can provide more direct measurements of properties of the older stellar population; we plan to report soon on a comprehensive UBV_RJHK imaging study of a subset of these galaxies in pairs.

We thank Jan Kleyna, Norman Grogan, and Daniel Koranyi for useful software and help with the data reduction procedures. We thank Lisa Kewley for the use of her abundance modeling code, and for many helpful comments; we also thank Eric Bell, Liese van Zee, Rob Kennicutt, and Rolf Jansen for helpful comments relating to this work. We are grateful to Perry Berlind and Mike Calkins for assistance with the spectroscopic observations and to Susan Tokarz for assistance with data reduction. Support for E. B. G. was provided by NASA through Hubble Fellowship grant #HST-HF-01135.01 awarded by the Space Telescope Science Institute, which is operated by the Association of Universities for Research in Astronomy, Inc., for NASA, under contract NAS 5-26555. The Smithsonian Institution supports the research of M. J. G. and S. J. K.

REFERENCES

- Abraham, R. G., Tanvir, N. R., Santiago, B. X., Ellis, R. S., Glazebrook, K., & van den Bergh, S. 1996, *MNRAS*, 279, 47
- Allende Prieto, C., Lambert, D. L., & Asplund, M. 2001, *ApJ*, 556, L63
- Andredakis, Y. C., & Sanders, R. H. 1994, *MNRAS*, 267, 283
- Barton, E. J., & van Zee, L. 2001, *ApJ*, 550, L35
- Barton, E. J., Geller, M. J., Bromley, B. C., van Zee, L., & Kenyon, S. J. 2001, *AJ*, 121, 625
- Barton, E. J., Geller, M. J., & Kenyon, S. J. 2000a, *ApJ*, 530, 660
- Barton, E. J., Kannappan, S. J., Kurtz, M. J., & Geller, M. J. 2000b, *PASP*, 112, 367
- Bell, E. F., & de Jong, R. S. 2000, *MNRAS*, 312, 497
- Bell, E. F., & de Jong, R. S. 2001, *ApJ*, 550, 212
- Bessell, M. S. 1990, *PASP*, 102, 1181
- Buser, G., & Kurucz, R. L. 1978, *A&A*, 70, 555
- Bruzual, A. G., & Charlot, S. in *AAS CD-ROM Series, Vol. 7, Astrophysics on Disc* (Washington: AAS) (GISSEL96)
- Calzetti, D., Kinney, A. L., & Storchi-Bergmann, T. 1994, *ApJ*, 429, 582
- Carollo, M. C. 1999, *ApJ*, 523, 566
- Carter, B. J., Fabricant, D. G., Geller, M. J., Kurtz, M. J., & McLean, B. 2001, *ApJ*, 559, 606
- Charlot, S., & Fall, S. M. 2000, *ApJ*, 539, 718
- Charlton, J. C., & Salpeter, E. E. 1991, *ApJ*, 375, 517
- Courteau, S. C. 1997, *AJ*, 114, 2402
- Diaferio, A., Kauffmann, G., Colberg, J. M., White, S. D. M. 1999, *MNRAS*, 307, 537
- Donzelli, C. J., & Pastoriza, M. G. 1997, *ApJS*, 111, 181
- Falco, E. E., Kurtz, M. J., Geller, M. J., Huchra, J. P., Peters, J., Berlind, P., Tokarz, S., & Elwell, B. 1999, *PASP*, 111, 438
- Heckman, T. M., Robert, C., Leitherer, C., Garnett, D. R., & van der Rydt, F. 1998, *ApJ*, 503, 646
- Hopkins, A. M., Connolly, A. J., Haarsma, D. B., & Cram, L. E. 2001, *ApJ*, 122, 288
- Jansen, R. A., Franx, M., Fabricant, D., & Caldwell, M. 2000, *ApJS*, 126, 271
- Jansen, R. A., Franx, M., & Fabricant, D. 2001, *ApJ*, 551, 825
- Jones, B., & Stein, W. A. 1989, *AJ*, 98, 1557
- Kauffmann, G., Colberg, J. M., Diaferio, A., & White, S. D. M. 1999, *MNRAS*, 303, 188
- Kauffmann, G., Colberg, J. M., Diaferio, A., & White, S. D. M. 1999, *MNRAS*, 307, 529
- Keel, W. C. 1993, *AJ*, 106, 1771
- Keel, W. C. 1996, *ApJS*, 106, 27
- Kennicutt, R. C., & Keel, W. C. 1984, *ApJ*, 279, L5
- Kennicutt, R. C., Jr., Keel, W. C., van der Hulst, J. M., Hummel, E., & Roettiger, K. A. 1987, *AJ*, 95, 5
- Kennicutt, R. C., Jr., Tamblyn, P., & Congdon, C. W. 1994, *ApJ*, 435, 22
- Kewley, L. J., & Dopita, M. J. 2002, *ApJS*, in press (astro-ph/0206495)
- Koo, D. C., Bershadsky, M. A., Wirth, G. D., Stanford, S. A., & Majewski, S. R., 1994, *ApJ*, 427, L9
- Landolt, A. U. 1992, *AJ*, 104, 340
- Larson, R. B., & Tinsley, B. M. 1978, *ApJ*, 219, 46
- Leitherer, C., et al. 1999, *ApJS*, 123, 3
- Liu, C. T., & Kennicutt, R. C., Jr. 1995a, *ApJ*, 450, 547
- Liu, C. T., & Kennicutt, R. C., Jr. 1995b, *ApJS*, 100, 325
- Madore, B. F. 1986, in *Spectral Evolution of Galaxies*, eds. C. Chiosi & A. Renzini (Reidel, Dordrecht), p. 97
- Mihos, J. C., & Hernquist, L. 1996, *ApJ*, 464, 641
- Miller, J. S., & Mathews, W. G. 1972, *ApJ*, 172, 593
- Miller, G. E., & Scalo, J. M. 1979, *ApJS*, 41, 513
- Peletier, R. F., & Balcells, M. 1996, *AJ*, 111, 2238
- Pfenniger, D., & Norman, C. 1990, *ApJ*, 363, 391
- Salpeter, E. E. 1955, *ApJ*, 121, 161
- Sekiguchi, K., & Wolstencroft, R. D. 1992, 255, 581
- Somerville, R. S., & Primack, J. R. 1999, *MNRAS*, 310, 1087
- Skillman, E. D., Kennicutt, R. C., & Hodge, P. W. 1989, *ApJ*, 347, 875
- Sullivan, M., et al. 2001, *ApJ*, 558, 72
- Thompson, R. I., Weymann, R. J., & Storrie-Lombardi, L. J. 2001, *ApJ*, 546, 694
- Tissera, P. B., Domínguez-Tenreiro, R., Scannapieco, & Sáiz, A. 2002, *MNRAS*, 333, 327
- Toomre, A., & Toomre, J. 1972, *ApJ*, 178, 623
- Tully, R. B., & Fisher, J. R. 1977, *A&A*, 54, 661
- Tully, R. B., Mould, J. R., & Aaronson, M. 1982, *ApJ*, 257, 527
- Tully, R. B., Pierce, M. J., Huang, J.-S., Saunders, W., Verheijen, M. A. W., & Witchalls, P. L. 1998, *AJ*, 115, 2264
- Tully, R. B., & Pierce, M. J. 2000, *ApJ*, 533, 744
- Veilleux, S., Kim, D.-C., Sanders, D. B., Mazzarella, J. M., & Soifer, B. T. 1995, *ApJS*, 98, 171
- Wang, B., & Heckman, T. M. 1996, *ApJ*, 457, 645
- Zombeck, M. V. 1990, *Handbook of Space Astronomy & Astrophysics, Second Edition* (Cambridge: Cambridge University Press)
- Zwicky, F. & Kowal, C. T. (1968). *Catalogue of Galaxies and Clusters of Galaxies* (California Institute of Technology, Pasadena). Vol. 6

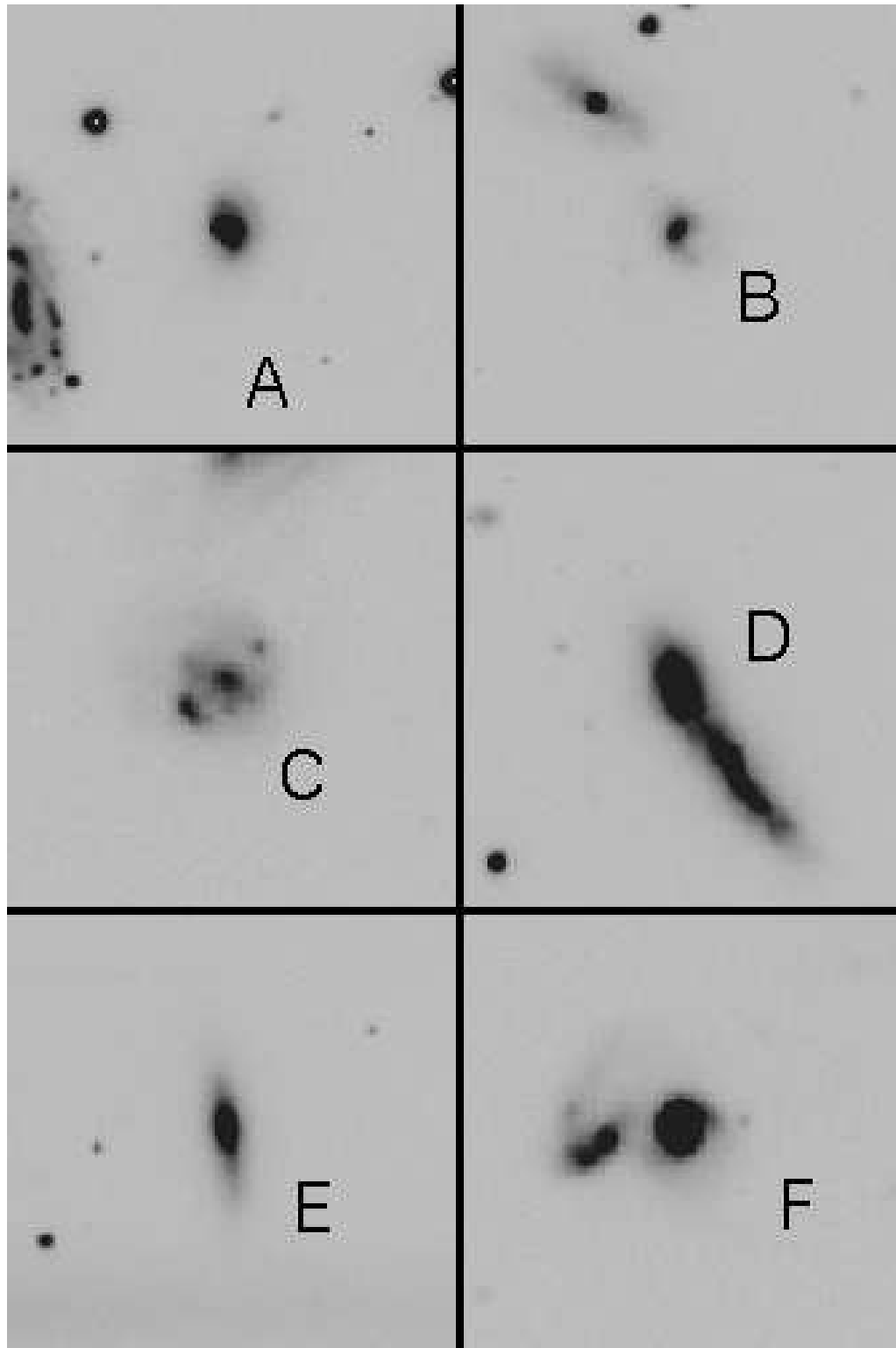


FIG. 23.— B -band images of the galaxies in Fig. 22. We center the images on the galaxies with nominal $s_R(t) > 1$. Galaxies “A” – “E” are UGC 312, IC 2338, NGC 3991-North, CGCG 132-062, and UGC 12011; they are labeled in Table 1. “D” refers to only the Northern galaxy in the close galaxy pair (*middle right*).

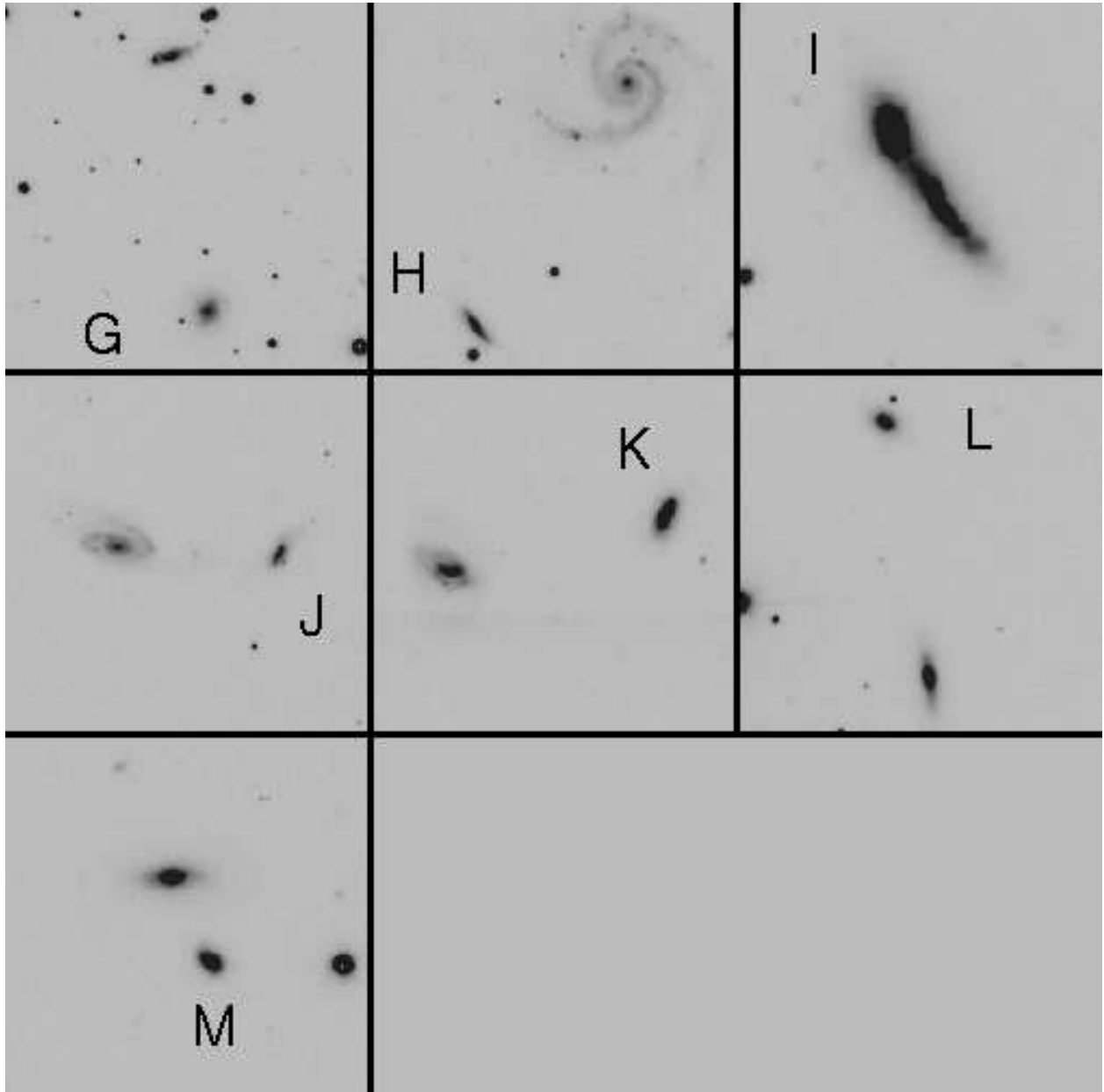


FIG. 24.— Pairs with one member selected based on $s_R(t)$, $EW(H\alpha)$, and ΔV to be near apogalacticon. Although some faint features are difficult to see in this figure, most of the pairs show signs of tidal interaction and/or lumpy star formation. The selected galaxies, “G” – “M”, are CGCG 059-050, CGCG 180-020, NGC 3991-North, UGC 07085-West, CGCG 217-024, CGCG 132-063, and UGC 12265-South; they are labeled in Table 1. (Note that “D” in Fig. 23 is the same galaxy as “I” here and “L” is the companion of “E”.)